JOURNAL OF GEOPHYSICAL RESEARCH, VOL. 112, D10103, doi:10.1029/2006JD007781, 2007

Water isotope expressions of intrinsic and forced variability in a coupled ocean-atmosphere model

Gavin A. Schmidt,[1] Allegra N. LeGrande,[1] and Georg Hoffmann[2]

Received 11 July 2006; revised 15 November 2006; accepted 10 January 2007; published 17 May 2007.

[1] Water isotopes provide a clear record of past climate variability but establishing their precise relationship to local or regional climate changes is the key to quantitative interpretations. We have incorporated water isotope tracers within the complete hydrological cycle of Goddard Institute for Space Studies coupled ocean-atmosphere model (ModelE) in order to assess these relationships. Using multicentennial simulations of the modern (preindustrial) and mid-Holocene (6 kyr BP) climate, we examine the internal variability and the forced response to orbital and greenhouse gas forcing. Modelled isotopic anomalies clearly reflect climatic changes and, particularly in the tropics, are more regionally coherent than the precipitation anomalies. Matches to observations at the mid-Holocene and over the instrumental period are good. We calculate water isotope-climate relationships for many patterns of intrinsic and for forced variability relevant to the Holocene, and we show that in general, calibrations depend on the nature of the climate change. Specifically, we examine relationships between isotopes in precipitation and local temperatures and precipitation amounts in the principal ice coring regions (Greenland, Antarctica, and the tropical Andes) and the seawater isotope-salinity gradients in the ocean. We suggest that isotope-based climate reconstructions based on spatial patterns and nonlocal calibrations will be more robust than interpretations based on local relationships.

Citation: Schmidt, G. A., A. N. LeGrande, and G. Hoffmann (2007), Water isotope expressions of intrinsic and forced variability in a coupled ocean-atmosphere model, *J. Geophys. Res.*, *112*, D10103, doi:10.1029/2006JD007781.

1. Introduction

[2] The ratios of oxygen and hydrogen isotopes in water have long been used as important tracers of the hydrologic cycle. These ratios are primarily affected by the fractionation occurring at changes of phase—principally during the liquid-to-vapor transition at evaporation or condensation. Since different freshwater sources in the climate system have different evaporation and condensation histories, they will in general have different isotopic ratios [reported in standard δ‰ units with respect to Vienna standard mean ocean water]. In particular, precipitation is more depleted than the water from which it evaporated, and high-latitude precipitation is considerably more depleted than rain in the midlatitudes.

[3] The diverse range of δ in natural freshwater can be useful in determining the proportion of freshwater from multiple sources. In the modern ocean, $\delta^{18}O_w$ has been used as a tracer for sea ice melt [*Macdonald et al.*, 1999, among others], glacial and river runoff [*Khatiwala et al.*, 1999; *Israelson and Buchardt*, 1999], deep-ocean-water masses [*Meredith et al.*, 1999], and deep-water formation processes [*Jacobs et al.*, 1985; *Toggweiler and Samuels*, 1995]. Coincidently, oxygen and hydrogen isotope signals related to the hydrologic cycle are among the most useful of paleoclimate proxies since they are preserved in many carbonate and ice-core records.

[4] General circulation models (GCMs) are an obvious tool with which to examine the relationship between the water isotopes and the climate since many (if not all) of the important physical processes are contained therein. Previously, these models have been used to simulate water isotope tracers separately in both the atmosphere [*Joussaume and Jouzel*, 1993; *Jouzel et al.*, 1991; *Hoffmann et al.*, 1998; *Noone and Simmonds*, 2002] and the ocean/ice system [*Schmidt*, 1998; *Delaygue et al.*, 2000; *Paul et al.*, 1999]. This paper presents some of the first results from fully coupled atmosphere-ocean simulations. The advantage of using a coupled model lies in the consistent simulation of the natural range of variability and also the ability to link changes in the different components of the model (for instance between the precipitation over land and the ocean variability). There are some similarities to this approach in atmospheric simulations that use a transient history of sea surface temperatures (SST) to force the model [e.g., *Hoffmann et al.*, 2003; *Vuille et al.*, 2003; *Brown et al.*, 2006]. However, there is reason to expect that the variability within a coupled system will be more physically consistent [*Bretherton and Battisti*, 2000; *Kushnir et al.*,

[1] NASA Goddard Institute for Space Studies and Center for Climate Systems Research, Columbia University, New York, New York, USA.
[2] Laboratoire des Sciences du Climat et de l'Environnement (LSCE), Orme des Merisiers, Gif-sur-Yvette, France.

0148-0227/07/2006JD007781$09.00

2002] even if it may not completely represent the full range of tropical Pacific variability for instance. These models can also generate isotopic boundary conditions for the past periods (such as the last glacial maximum) that are otherwise unavailable.

[5] The key issue that we address in this paper is how variations in oxygen and hydrogen isotopes in water are related to climate and, therefore, how their past variability (as recorded in climate proxies such as ice cores, corals, lake and deep sea sediment, tree ring cellulose, speleothems, etc.) might be interpreted. Hereafter whenever we refer to isotopes, we imply the oxygen and hydrogen isotopologues of water molecules.

[6] Most interpretations of isotopic time series have followed initial observations that mid- and high-latitude isotope ratios in precipitation are highly correlated to local temperatures, while in the tropics, ratios are more related to the local precipitation "amount effect" [*Dansgaard*, 1964; *Rozanski et al.*, 1993]. However, the quantitative aspects of these relationships have been a matter of some debate. In lieu of the better information, it was initially supposed that present-day correlations between climate and isotope proxies at a number of different sites (the "spatial" relationship) were a good approximation for the relationship over time at any particular site (the "temporal" relationship). For instance, the gradient between the annual mean oxygen isotope ratio in precipitation ($\delta^{18}O_p$) and annual mean temperature from different observing sites implies a calibration of about 0.7‰/°C in Greenland ice cores [*Dansgaard*, 1964]. However, as other proxies have become available for cross-checking [i.e., *Dahl-Jensen et al.*, 1998], and models become more capable [*Werner et al.*, 2000], the actual calibration over glacial-to-interglacial timescales appears to only be half as large. Thus the assumption that the spatial gradient is a good approximation to the temporal gradient has been shown not to be valid in the general case (although it still appears reasonable for Antarctic ice cores [*Jouzel et al.*, 2003]). Similar assumptions made regarding $\delta^{18}O_w$ and salinity [*Duplessy et al.*, 1993] may have similar problems [*Schmidt*, 1999b; *Rohling and Bigg*, 1998].

[7] Some isotope records have been interpreted in terms of a source region effect (i.e., a nonlocal interpretation). Specifically, in ice cores where both deuterium and oxygen isotope ratios can be measured, the difference (expressed as the deuterium excess: d-excess = $\delta D - 8\delta^{18}O$) has been related to temperatures at the evaporative source region [*Ciais et al.*, 1994; *Vimeux et al.*, 2001]. Tropical records in ice cores and speleothems have also been interpreted as regional signals of the Intertropical Convergence Zone (ITCZ) or monsoonal changes [*Hoffmann et al.*, 2003; *Vuille et al.*, 2003; *Wang et al.*, 2005].

[8] But how robust are these relationships? How might they vary depending on the timescale or the nature of the climate change? To attempt to answer these and other questions, we look at the internal variations on interannual and decadal scales in the long quasi-steady coupled integrations of the climate system. We also examine the forced response associated with long-term orbital forcing and greenhouse gas changes [comparing the mid-Holocene (MH) (6 kyr BP) and preindustrial (PI) climates]. Using these comparisons, we examine the variability of the temporal gradients (and hence the isotope-to-climate inversion) as a function of timescale and forcing mechanism. Additionally, for key locations (such as for the polar ice coring sites), we regress the simulated isotopic records there onto the patterns of climate variability [in SST, sea-level pressure (SLP), precipitation, etc.] to assess the nature of possible nonlocal influences on an individual site.

2. Model Description

2.1. Coupled Model

[9] The model used is the coupled GISS ModelE-R which was used in simulations in support of the IPCC AR4. The atmospheric component used in this study is described in the study of *Schmidt et al.* [2006] and is similar to the SI2000 version described in the work of *Hansen et al.* [2002], with improvements to the cloud physics, surface boundary layer, and stratospheric circulation. The model has 20 vertical levels up to 0.1 hPa in height (significantly higher than most previous model versions).

[10] The ocean component is the Russell ocean model [*Russell et al.*, 1995, 2000; *Liu et al.*, 2003] which is mass conserving and uses "natural" boundary conditions at the free surface (freshwater, heat, and salt fluxes). It uses a Gent-McWilliams mesoscale eddy parameterization with variable coefficients [*Gent and McWilliams*, 1990; *Visbeck et al.*, 1997]. Vertical mixing uses the KPP scheme [*Large et al.*, 1994], and horizontal momentum diffusion follows the prescription of *Wajsowicz* [1993]. Sea ice is modelled using a four-layer thermodynamic scheme and is advected using the viscous-plastic ice rheology [*Zhang and Rothrock*, 2000; *Liu et al.*, 2003; *Schmidt et al.*, 2004a].

[11] Both ocean and atmosphere models are run at the same, relatively coarse, $4° \times 5°$ resolution, and the coupling is synchronous (once every 30 minutes). Higher-order upstream schemes [*Russell and Lerner*, 1981; *Prather*, 1986] are used to advect tracers in the atmosphere and ocean in a positive definite, conserving, highly nondiffusive way.

2.2. Isotope Tracers

[12] Some of the earliest experiments using water isotope tracers in atmospheric models were performed using GISS Model II [*Jouzel et al.*, 1987, 1991; *Charles et al.*, 1994; *Cole et al.*, 1999]. However, much new physics has been incorporated into the GISS models since then, and these have an important effect on the isotope signal as described more fully in the paper of *Schmidt et al.* [2005]. In particular, we have upgraded the isotopes to follow the physics intrinsic to the state-of-the-art prognostic cloud liquid water and convection schemes [*Del Genio et al.*, 1996; *Yao and Del Genio*, 1989; *Del Genio et al.*, 2005] now used in the GCM. Many important processes (such as the amount of downdrafting and entrainment), which were previously estimated independently of the cloud scheme, are now treated explicitly albeit in a parameterized fashion.

[13] We use a parameterized supersaturation function $S = 1 - 0.004 * T$ [where T is temperature (°C)] for the kinetic effect that occurs when condensing vapor to ice crystals in clouds. The value is chosen as in previous work to improve the simulation of the deuterium excess in Antarctic precipitation [*Schmidt et al.*, 2005]. There is some uncertainty in the relative isotopic diffusion coefficients used in estimating the

kinetic fractionation during evaporation and condensation [*Cappa et al.*, 2003]. Sensitivity tests using the atmosphere-only model showed significant deterioration in the deuterium-excess signal in precipitation as a function of the suggested new values [*Schmidt et al.*, 2005]. We intend to reexamine the basis of these calculations using a fuller calculation of the surface evaporative process [*Brutsaert*, 1982] using isotopically varying Schmidt numbers as opposed to a parameterization such as that of *Merlivat and Jouzel* [1979]. This will be reported in future work.

[14] In the land surface, tracers are contained within the three-layer snow model [*Lynch-Stieglitz*, 1994] and the six-layer soil water model [*Rosenzweig and Abramopoulos*, 1997]. Evapotranspiration occurs with no fractionation and takes water and tracers from the relevant root depth. Fractionation occurs when evaporating water from bare soil and from the canopy [*Aleinov and Schmidt*, 2006]. In lakes, tracers in the upper mixed layer and deep layer are prognostic and depend consistently on runoff, evaporation, precipitation, and inflow/outflow. River outflow to the ocean has a consistent isotopic signature based on the integrated upstream precipitation, evaporation, and runoff.

[15] In sea ice, isotopic tracers are included within the four-layer snow and ice scheme and are transported by the ice dynamics. Meltwater (from the surface or through lateral and basal melting) has the same isotopic ratio as the ice from which it comes. Formation of ice in the open ocean, or at the ocean-ice interface, fractionates, with the ice being 3.5‰ (δ^{18}O) or 20.8‰ (δD) more enriched than the water [*Schmidt*, 1999b].

[16] In the ocean, tracers are affected by all of the subgrid-scale processes (isopycnal mixing, mesoscale eddy-induced mixing, diapycnal diffusion schemes, straits, etc.). All freshwater fluxes (precipitation, river and glacial runoff, evaporation, sea ice formation, and melting) are tagged isotopically. Antarctic and Greenland glacial runoff is assumed to have a -20‰ δ^{18}O value (-160‰ δD). We therefore simulate all of the processes that affect the seawater isotope signal in a physically consistent way. Of course, this does not guarantee accurate simulations of reality, but it does allow us to examine in detail the interactions between the different processes.

[17] We note that the use of a free surface and natural freshwater flux boundary conditions at the ocean surface (as opposed to a rigid lid and ''equivalent'' salt fluxes) greatly simplifies the implementation of isotopic fluxes and allows for a fully prognostic calculation of isotope-salinity relationships.

2.3. Other Simulations

[18] In order to assess the utility of the coupled model simulations of isotope variability, it is useful to compare some fields with isotope-enabled simulations that have more realistic ocean temperatures than the coupled model provides. Specifically, we reference the equilibrium present-day simulations described in the work of *Schmidt et al.* [2005] and the twentieth-century transient simulations performed with observed changes in SST and sea ice extent from 1880 to 2000 [*Rayner et al.*, 2003] described in the paper of *Aleinov and Schmidt* [2006]. In both cases, the same atmospheric component as described here was used, with surface ocean isotope fields set as constants (δ^{18}O = δD = 0‰).

[19] Additionally, since the North Atlantic Ocean variability is relatively small in the control runs of the coupled model, we analyze simulations of the 8.2-kyr BP event [*LeGrande et al.*, 2006], which have larger variations (up to 60% decreases) in the North Atlantic overturning circulation.

3. Coupled Climatology: Preindustrial Period

[20] We present results from a control coupled simulation that was started from the temperature and salinity observations of *Levitus et al.* [1994] and run with 1880 atmospheric composition [*Hansen et al.*, 2005]. Ocean isotopes were initialized using a zonal profile based on observed profiles [*Schmidt*, 1998]. After a multicentury spin-up (100 years without isotope tracers and then another 600 years with isotopes included), the model has stabilized in the atmosphere and over most of the ocean. There are some remaining drifts (0.1°C/century), but these are relatively small and have little effect on the other surface features. We analyze the results from the last 200 years of this simulation for the climatology and the interannual and decadal variability.

[21] We compare the PI simulation to observations of isotope ratios in precipitation and the ocean from the late twentieth century due to the absence of observations for PI isotopic ratios (except in paleoproxy records). Transient experiments with an atmosphere-only model [*Aleinov and Schmidt*, 2006] indicate that the changes in isotopic fields over the twentieth century are relatively small, and the discrepancies between the model and the observations seen here are much larger than any possible transient signal.

[22] Some global mean quantities are of particular interest for isotopes. The mean precipitation rate is 3.0 mm/day, slightly higher than observed ($\sim$2.7 mm/day), although there is a significant uncertainty among data sets [*Huffman et al.*, 1997; *Xie and Arkin*, 1997]. Of that, just over 60% is precipitation associated with moist convection, primarily in the tropics. The global mean $\delta^{18}O_p$ is -6.0‰. This is more depleted than previously assumed by *Craig and Gordon* [1965] who estimated a value of -4‰, but this is consistent with other modelling studies [*Hoffmann et al.*, 1998]. The principal difference is that Craig and Gordon assumed too high a value for the isotope ratio in tropical precipitation (20°S–20°N approximately -2‰) compared with the approximately -5‰ seen here. The mean surface relative humidity is close to 80%, and the mean isotopic ratio in the surface water vapor $\delta^{18}O_v$ is -13‰.

[23] Figure 1a shows the isotopic ratio in precipitation. This pattern is highly correlated (area-weighted $r^2 = 0.71$) to the observed fields [*Rozanski et al.*, 1993; *International Atomic Energy Agency*, 2001] and again is similar to that seen in other models [*Jouzel et al.*, 1987; *Hoffmann et al.*, 1998], including the atmosphere-only version of this model [*Schmidt et al.*, 2005]. Despite the offsets of the coupled climate from the observed, the match to the isotopes is better in the coupled model (higher correlation, lower bias though a slightly larger RMS error) than in the atmosphere-only model.

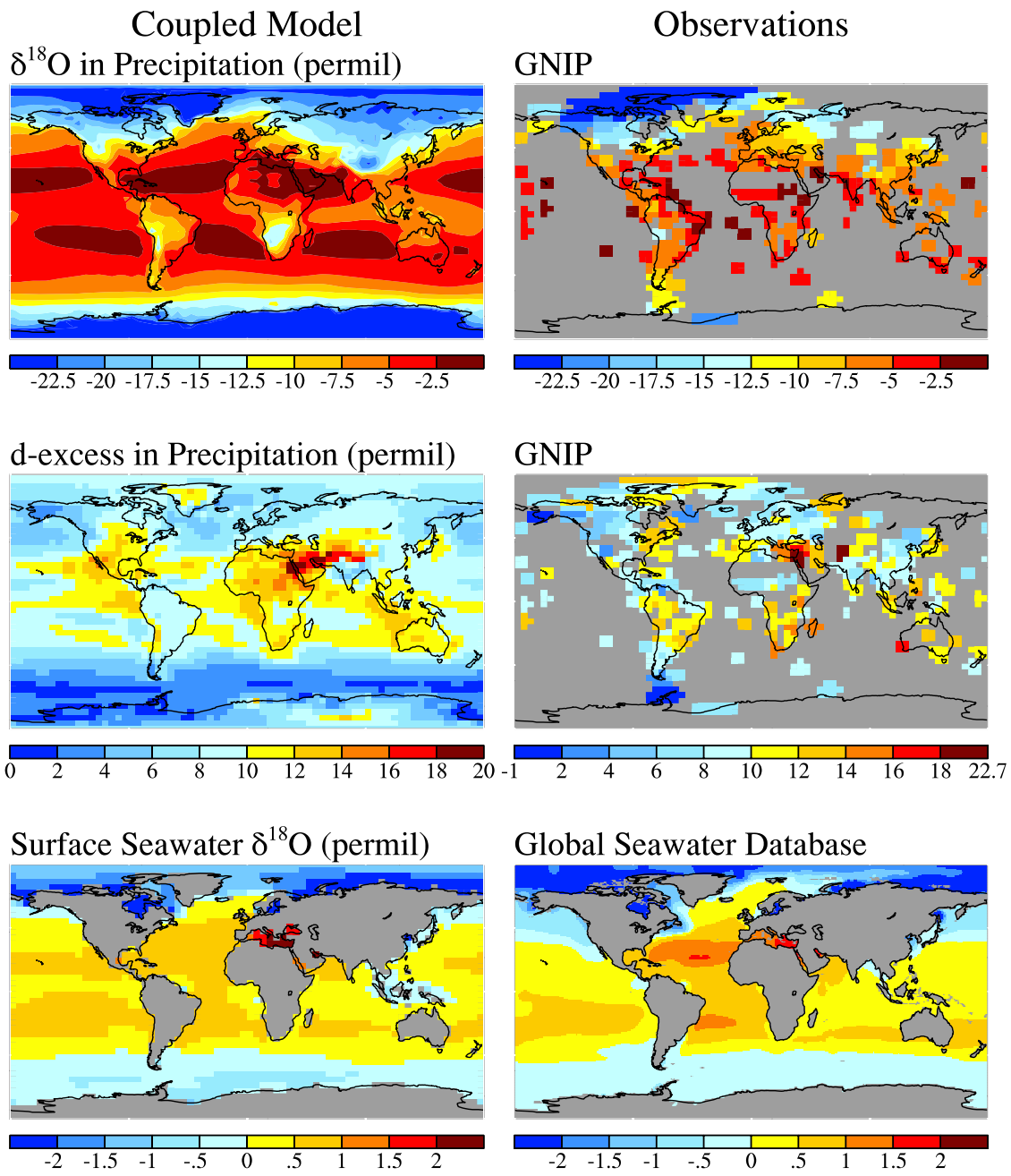

Figure 1. (top row) Modelled annual mean (PI) isotopic ratio in precipitation ($\delta^{18}O_p$)compared to the GNIP climatology [*IAEA*, 2001]. (middle) Same but for d-excess. (bottom row) Modelled isotopic ration ($\delta^{18}O_w$) in surface seawater compared to the Global Seawater Oxygen-18 Database [*Schmidt et al.*, 1999; *LeGrande and Schmidt*, 2006].

[24] Using both deuterium and $\delta^{18}O$ tracers, we compute the d-excess in all the water reservoirs. The d-excess field in precipitation is less well observed, and less well modelled ($r^2 = 0.24$), than the isotopic ratios, but the general pattern is reasonably simulated (Figure 1b). The precipitation values show a number of clear similarities with observations, in particular the small d-excess values over the Southern Ocean. Tropical values show the greatest offsets. In line with the importance of surface source conditions, the coupled model simulation is slightly worse than the atmospheric model with observed SST. However, one improvement seen in the coupled model over the atmosphere-only model [*Schmidt et al.*, 2005] is the higher d-excess values seen around the Mediterranean and the Middle East. This may be due to warmer temperatures in the coupled model or higher variability, but this cannot be due to a source water effect since the Mediterranean d-excess value is actually lower than in the atmospheric model.

[25] The isotopic ratio in zonal mean atmospheric water vapor (not shown) is very similar to that seen in the atmosphere-only model [*Schmidt et al.*, 2005]. The Hadley circulation has a January maximum overturning of 205 ×

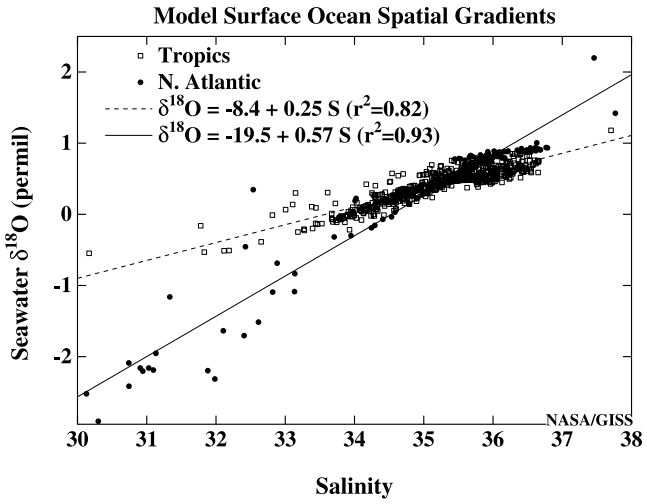

Figure 2. Climatological relationship between seawater $\delta^{18}O_w$ and salinity in the North Atlantic extratropics and the global tropical ocean (annual means in the PI simulation).

10^9 kg s^{-1} compared to the atmosphere-only model value of 179×10^9 kg s^{-1} and an observational range of $170-200 \times 10^9$ kg s^{-1}. Hence the minimum values in the lower stratosphere are slightly lower than in the atmosphere-only simulations (for δD, approximately −680‰ compared to approximately −670‰ in the atmospheric GCM).

[26] Comparison of the surface ocean $\delta^{18}O_w$ (Figure 1c) to a compilation of surface ocean observations [*Schmidt et al.*, 1999] (gridded data from the work of *LeGrande and Schmidt* [2006]) show some pleasing similarities (area-weighted correlation $r^2 = 0.77$). The contrast between the evaporative zones and the midlatitudes is well captured, as is the contrast between the Atlantic and the Pacific basins. Regionally, there are some obvious deficiencies; in particular, the isotopic signal of the North Atlantic drift does not penetrate as far north as observed, and the evaporative region maxima in the Atlantic are too muted and too zonal. However, the overall pattern is significantly better than the ocean-only simulations previously described [*Schmidt*, 1998, 1999b]. This is mainly due to the effect of more realistic ocean-atmosphere feedbacks in the coupled model and the more robust North Atlantic overturning stream function in this version of the model. Most of the remaining problems seem to be related to known deficiencies in the coupled model (too little subtropical evaporation, etc.) rather than the isotope physics.

[27] The net northward flux of atmospheric water out of the tropics (at 28°N) has a mean isotopic ratio of −16.5‰, close to the mean freshwater end-member for the North Atlantic in the model (−19‰, Figure 2) and compares favorably to the −18‰ seen in observations [*Östlund et al.*, 1987]. The modelled salinity-δ^{18}O slopes (per mille per practical salinity unit) are also similar to observations: 0.57 compared with 0.53 in the North Atlantic and 0.24 compared with 0.30 in the tropics [*Schmidt*, 1999a].

[28] Observations of d-excess in surface ocean water are not as widespread as for $\delta^{18}O_w$, but the data that exist are plotted in Figure 3 (as a function of δ^{18}O). This ocean data may be sufficient to help resolve ongoing issues in modelling the deuterium excess [*Cappa et al.*, 2003; *Schmidt et al.*, 2005] since they must be consistent with the independently collected rainfall data. The model is slightly enriched in d-excess compared to the bulk of the observations, but it shows a similar increase in d-excess in fresher water. The one area where the modelled d-excess significantly disagrees with observations is in the Mediterranean Sea, where the data show almost no change in as δD as δ^{18}O varies [*Gat et al.*, 1996]. Modelled values in this region do not show any anomalous behavior, and so these results are slightly enigmatic. *Gat et al.* [1996] suggested that this pattern was a result of repeated evaporation/precipitation events in very dry air in the region, and so the model result may be a function of insufficient evaporation or conceivably of too much mixing with non-Mediterranean air. Further investigation of this mismatch would be useful but it is beyond the scope of this paper.

[29] Hereafter, we focus predominantly on oxygen isotopes for clarity, but the results for deuterium are very similar after an appropriate scaling.

4. Intrinsic Variability

[30] Within a coupled control run, the variability on the interannual, decadal, and multidecadal timescales is self-generated by the chaotic dynamics of the atmosphere and through ocean-atmosphere interactions. Because principally of the thermal inertia and advection timescales of the oceans, this variability can have significant decadal and longer spectral power. We note that most current models of the ocean incorporated into the coupled models (and in particular the model used here) do not resolve the mesoscale eddy field and therefore do not generate their own "noise".

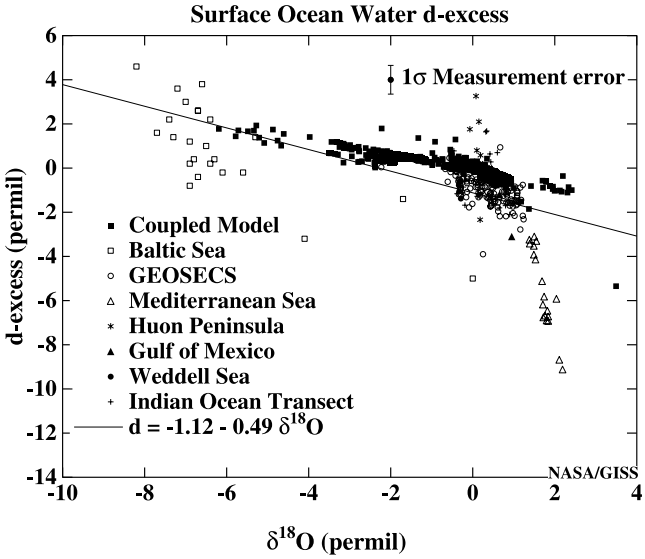

Figure 3. Annual mean PI results and observed d-excess in surface ocean waters. Observations from Baltic Sea [*Fröhlich et al.*, 1988], Mediterranean [*Gat et al.*, 1996], GEOSECS (Atlantic, Pacific, and Indian Ocean sections) [*Östlund et al.*, 1987], Indian Ocean [*Duplessy*, 1970; *Delaygue et al.*, 2000], Gulf of Mexico [*Yobbi*, 1992], Weddell Sea [*Weiss et al.*, 1979], and Huon Peninsula [*Aharon and Chappell*, 1986]. The solid line shows the correlation from all surface data.

We focus here on modes of internal variability, which have been of particular interest in paleoclimate studies.

[31] We examine the variability on two specific timescales (interannual and decadal) and in a number of phenomena—specifically the isotopic expression of the annular modes, tropical SST variability, and North Atlantic thermohaline circulation variability. We note that since the GCM has relatively coarse resolution, interannual variability in the tropical Pacific is significantly reduced compared to observations. While this underestimation clearly limits the usefulness of the variability results in the tropics, the results shown here may still be of partial use despite the smaller magnitude signal than observed (see below for more details).

[32] For each of the patterns of variability highlighted, we derive an index of that mode using a principal component analysis or by simply picking out a relevant diagnostic in the model, and we regress the isotopic patterns (principally the isotopic ratios in precipitation and surface water) to determine the isotopic signatures of that pattern on the different timescales. All regression and correlation maps shown here are masked so that only values significant at the 95% level are shown.

4.1. Annular Modes

[33] For both hemispheres, we take the monthly mean data over the last 100 years of the coupled control run and calculate a model annular mode index from the leading empirical orthogonal function (EOF) of the monthly SLP anomalies [*Thompson and Wallace*, 1998; *Shindell et al.*, 2001]. In the Northern Hemisphere (NH), we use only the winter months (November–April) to define the northern annular mode (NAM). In the south, we utilized all monthly data to analogously define the southern annular mode (SAM) but use only 80 years due to computational constraints. Each index is scaled so that it represents the mean SLP deficit poleward of 60°, i.e., a +1 in the index implies a mean SLP change of −1 hPa over the pole and a more enhanced (positive) phase of the pattern. Traditional definitions of the North Atlantic oscillation are highly correlated to the NAM index and, for all practical purposes, can be regarded as synonymous. The NAM index captures 19% of the variance in SLP compared with 21% in the observations and 22% in the atmosphere-only model. In the Southern Hemisphere (SH), SAM-related variability explains around 30% of the variance similar to the observations and atmospheric model [*Miller et al.*, 2006].

[34] We correlate these monthly indices to the anomalies in the temperature, precipitation, and isotope fields (including the deuterium excess in precipitation) in order to diagnose the monthly to interannual variability associated with these modes. The temperature and precipitation correlations resemble those seen in observations and other models [*Thompson and Wallace*, 1998; *Shindell et al.*, 2001]. As expected, the pattern of NH $\delta^{18}O_p$ variability (Figure 4) closely resembles patterns of temperature variability at least in the North Atlantic and Europe where onshore advection is the dominant feature. Further afield (North Africa, tropical Atlantic), the connections are not as clear. The d-excess is more strongly correlated to the NAM index than the $\delta^{18}O_p$ although in the subtropics, the impact of coincident precipitation changes clearly affects that correlation.

[35] In the SH, temperature correlations to the SAM index are weak, reflecting the zonal nature of the temperature patterns, but are surprisingly high for precipitation (Figure 5). The precipitation increases in areas of higher zonal winds and decreases on the continent. The $\delta^{18}O_p$ field approximates the temperature pattern (as seen in observations [*Schneider et al.*, 2006]), but interestingly, the d-excess signal is strongly negatively correlated to SAM over the bulk of the Antarctic region. Results for all fields are similar when using decadal means over a 200-year period (not shown).

4.2. Tropical Variability

[36] As stated above, tropical variability in the coupled model is significantly less than observed (the standard deviation of monthly tropical surface air temperature (SAT) anomalies is about 80% of the observed for simulations of the late twentieth century [*Santer et al.*, 2005]). Additionally, SST variability in the Niño-3 region is around one fifth of that observed. We therefore use results from the twentieth-century simulations [*Aleinov and Schmidt*, 2006], which used observed SST and sea ice variations, to compare with the coupled model results to see whether the teleconnection patterns are robust.

[37] We perform an EOF analysis on the last 80 years of detrended monthly tropical SST anomalies (Figure 6). The leading EOF explains 44% of the tropical SST variance in the twentieth-century simulation but only 10% in the coupled model. However, in both cases, the patterns resemble classic El Niño patterns (rather surprisingly in the case of the coupled model), including an Indian Ocean teleconnection, though the sign of the covariability in the Atlantic is reversed in the coupled model. The pattern of regression in the isotopes is very similar in both cases over much of the globe (spatial r^2 = 0.43 in the tropics, 0.37 globally). As the East Pacific warms, convection (and more depleted $\delta^{18}O_p$) moves east [*Brown et al.*, 2006], while rainfall over the West Pacific warm pool and the Amazon is suppressed with more enriched isotopes as observed [*Hoffmann*, 2003; *Vuille et al.*, 2003]. Regressions in the Amazon/Andes region are about 1 to 2‰/°C change in the Niño-3 region, which are similar to the observations (i.e., ∼1.6‰/°C at Sajama (18°S 69°W) [*Bradley et al.*, 2003]). On the decadal timescale, both the EOFs and the teleconnections are similar (not shown).

5. Mid-Holocene Simulation

[38] The mid-Holocene (defined here as 6 kyr BP) has long been a target for modelling and paleoclimate data-model comparison [*Braconnot et al.*, 1999; *Joussaume et al.*, 1999]. The principle forcing change from the PI is due to the orbital configuration (precession) [*Berger*, 1978] that leads to increased NH summer insolation and slightly reduced tropical values but with very small changes in the global mean. There are additionally some significant greenhouse gas changes (decreases of 14 ppm in CO_2, 240 ppb in CH_4, and 50 ppb in N_2O) [*Etheridge et al.*, 1996; *Indermuhle et al.*, 1999] and some vegetation changes for this period [*Prentice and Webb*, 1998]. In the simulation

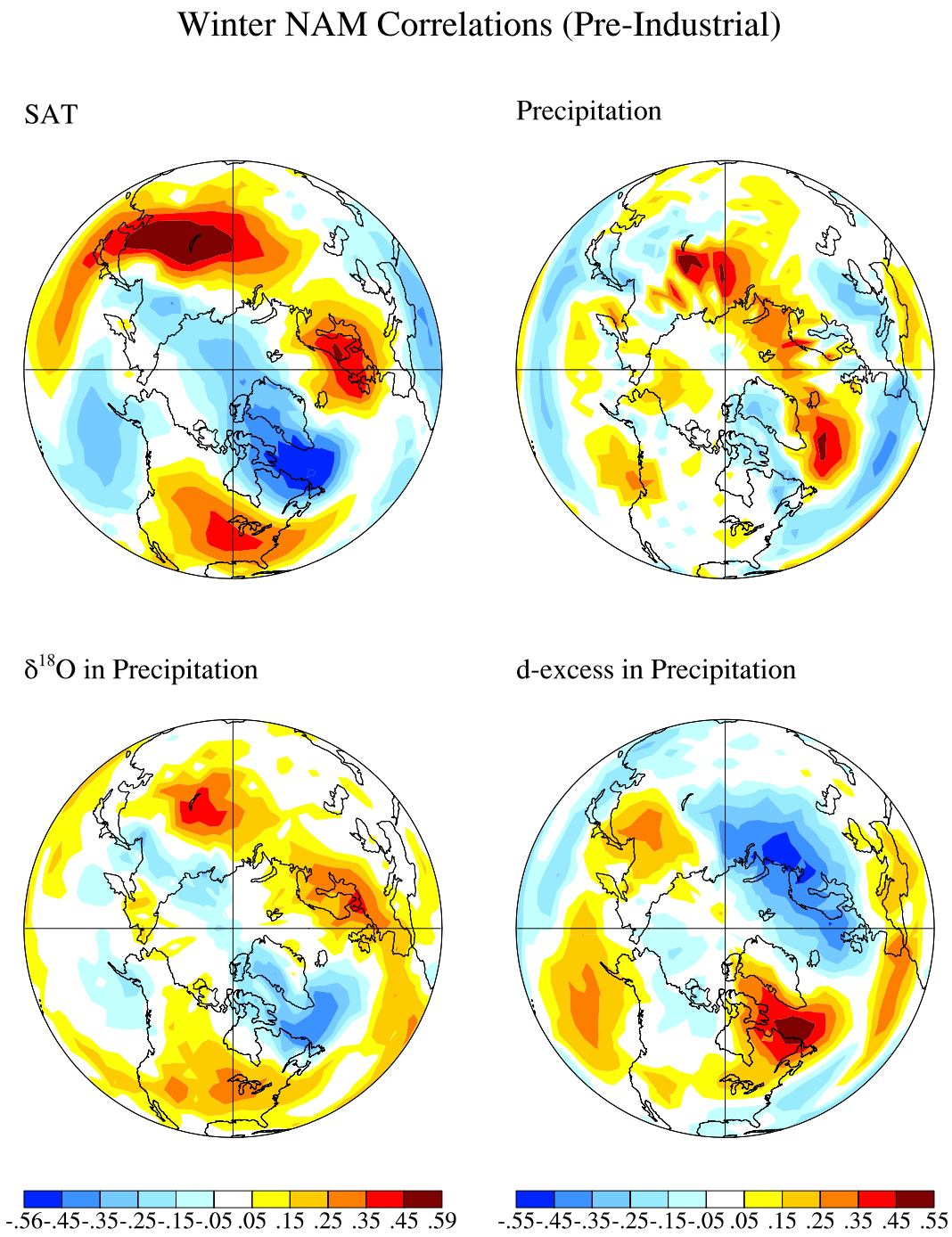

Figure 4. Correlations between the NAM index and the temperature, precipitation, and δ^{18}O d-excess using a zero-lag monthly varying index (winter months only) in the PI simulation.

described here, we use both the orbital and the greenhouse gas changes (but with modern vegetation) and allowed the coupled model 500 years to adjust. Results are taken from the last 100 years of the simulation.

[39] In agreement with previous results with coupled models [e.g., *Hewitt and Mitchell*, 1998; *Liu et al.*, 2000], the MH is characterized by a northward shift of rainfall in the subtropics and warmer summer temperatures in the northern high latitudes (Figure 7). The SAT in the annual mean is cooler by about 0.9°C, of which half is related to the greenhouse gas forcing of around -0.58 W/m^2, which would cool the surface by around 0.44°C in the atmosphere-only model (sensitivity of 2.7°C for the doubled CO_2). Orbital forcing alone does not significantly affect the mean temperature in an atmosphere-only run [*Schmidt et al.*, 2004b], and so the residual cooling is either a feedback within the coupled model or a part of a long-term transient related to the climate model drift. The spatial patterns of change in precipitation and isotope ratios are more robust than the global mean temperature change, and so we focus on these results here.

[40] Globally, moist-convective precipitation is slightly decreased in the MH, and the total column water is 7% less. In the ocean, there is a slight increase in the North Atlantic

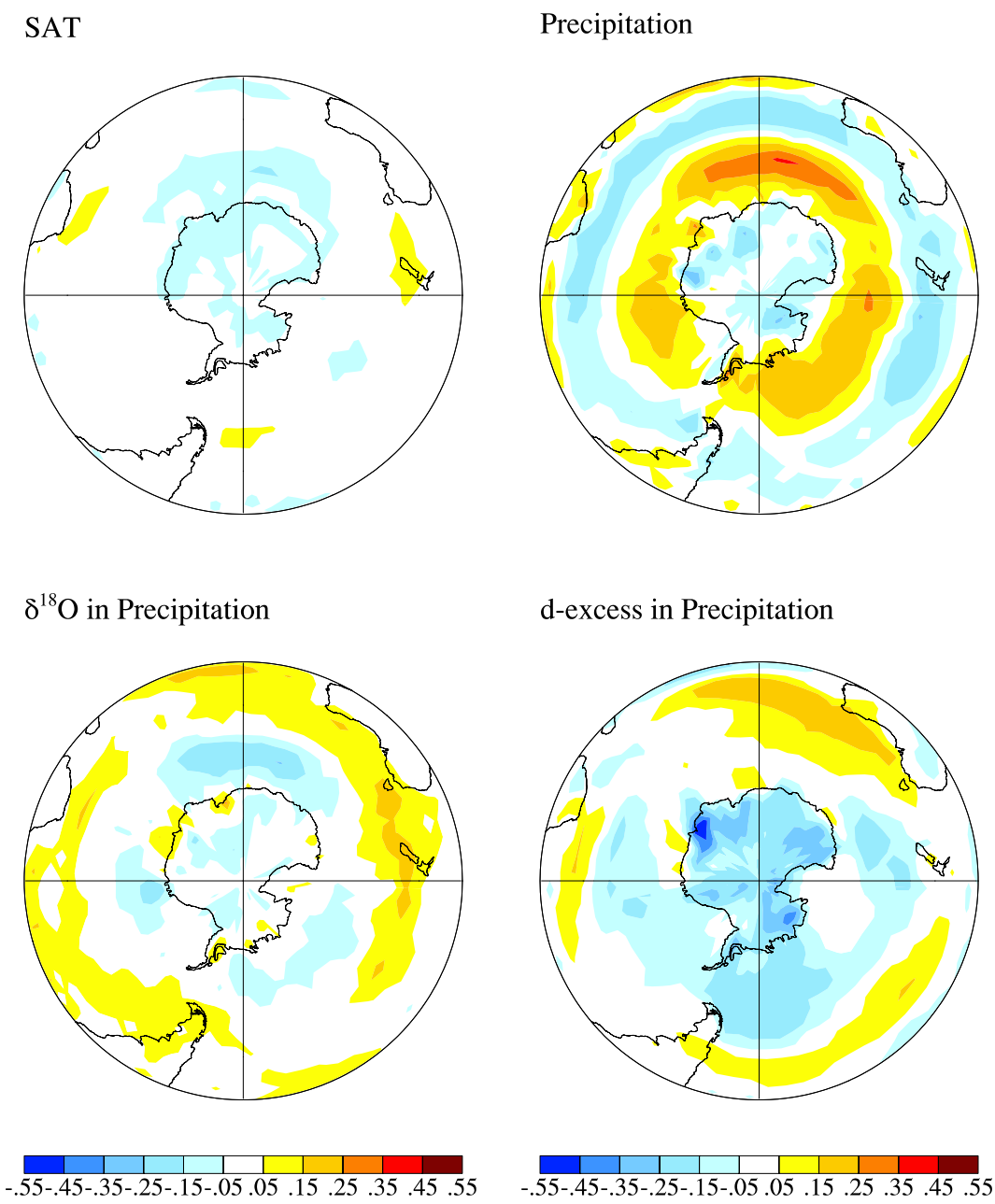

Figure 5. As in Figure 4, but for the SAM (all months).

Deep Water (NADW) index (defined as the value of the Atlantic basin averaged overturning mass stream function at 48°N and 900 m depth) to 21.4 Sv compared to 19.1 Sv in the PI simulation, enhancing the relative increase in the Northern Hemisphere SST slightly.

[41] There is a strong land-ocean contrast in the response of the rainfall, with significantly more precipitation over Africa and Asia and less over the tropical oceans, particularly the West Pacific warm pool. This is predominantly an NH summer signal although January precipitation is reduced on the equator as well. Moist convection is enhanced over the continents at the expense of the oceans, in particular the Pacific. The surface pattern of $\delta^{18}O_w$ reflects the changes in evaporation and runoff seen in the atmospheric diagnostics (Figure 7d). In particular, Atlantic and Indian tropical waters are more depleted in $\delta^{18}O_w$ (and enriched in d-excess, not shown) in response to reduced evaporation (and enhanced continental runoff in the Bay of Bengal). Conversely, the Pacific sector is significantly enriched in $\delta^{18}O_w$ (and in salinity) compared to the rest of the tropics.

[42] Examining the moisture fluxes in the model shows that there is an enhanced water divergence at the equator, increased vapor export from the Pacific into the Indian

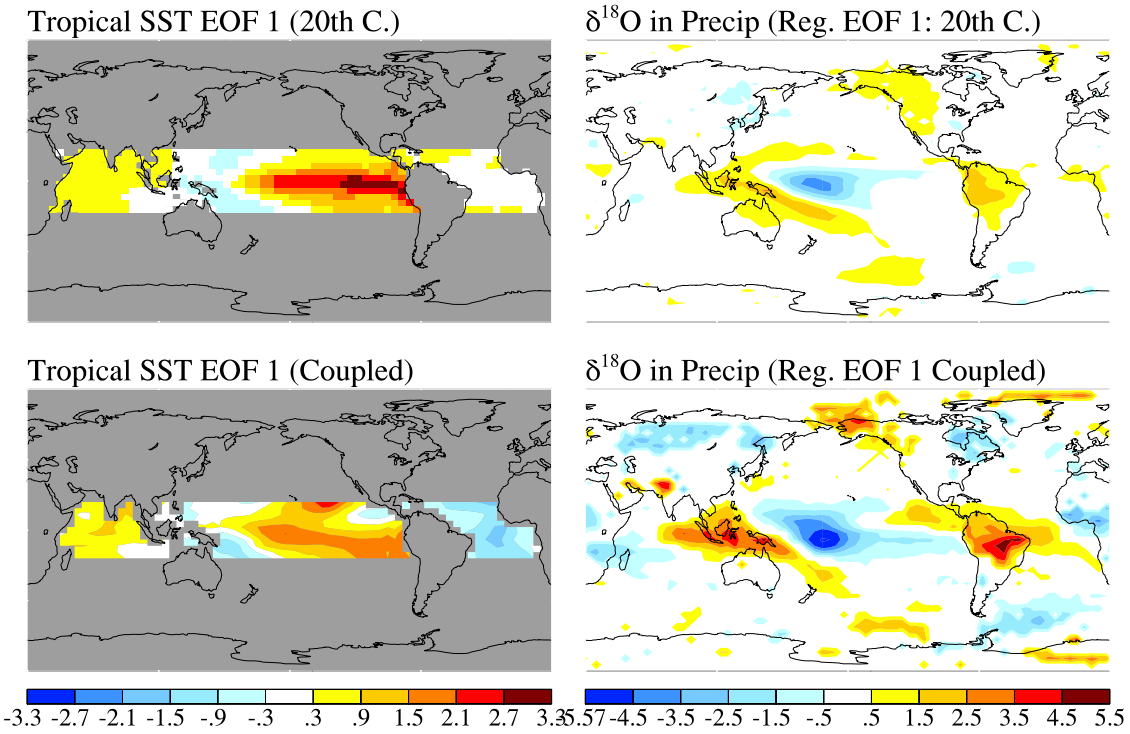

Figure 6. The leading EOFs in the twentieth-century tropical SST [*Aleinov and Schmidt*, 2006] (top row) and the PI simulation (bottom row) and the regressions against $\delta^{18}O_p$. The EOF patterns are normalized to have a mean SST of 1°C, and the regressions are in units of per mille per degree Celsius with respect to that mean.

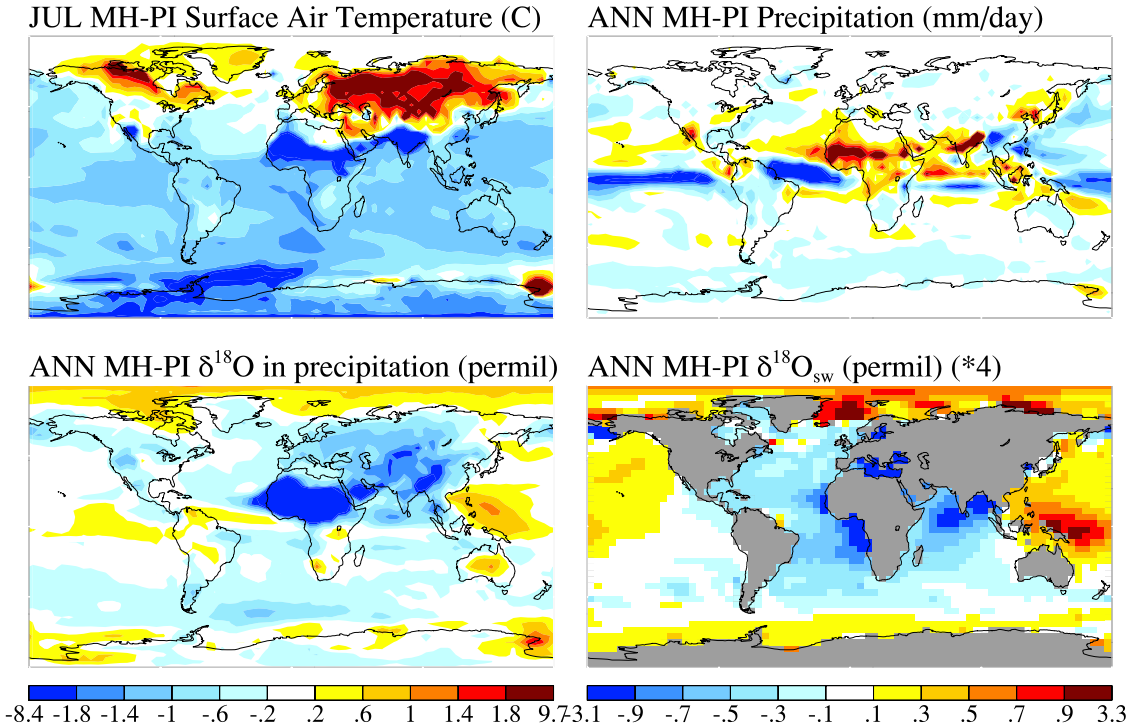

Figure 7. Mean differences between the MH and the PI simulations: July SAT (top left), precipitation (top right), $\delta^{18}O_p$ (bottom left), and annual mean surface seawater $\delta^{18}O$ (bottom right) (multiplied by 4 for scaling purposes).

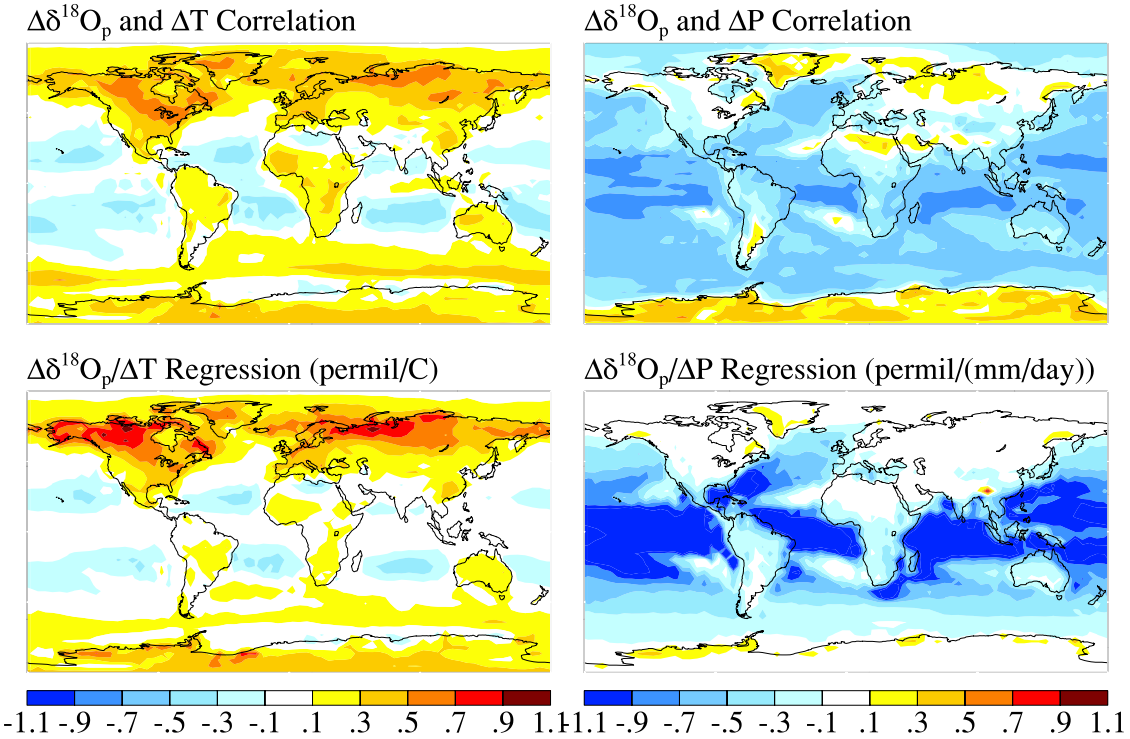

Figure 8. Local correlations and regressions of $\delta^{18}O_p$ to SAT (left) and precipitation (right) for the interannual variability (using monthly anomalies) in the coupled model. All shown values are significant at the 95% level.

Ocean, plus a decreased flux from the Atlantic into the Pacific (across the isthmus of Panama). All of these factors drive increasing salinification/enrichment of the tropical Pacific at the expense of freshening/depletion in the Atlantic and Indian oceans.

[43] In July, there is a dipole in the response of the Indian and East Asian monsoons, with a significantly enhanced rainfall over India but a reduced rainfall over China. The pattern in the isotopes, however, is a uniform 1–2‰ depletion across the region. This is in very good agreement with speleothem records from Dongge [*Wang et al.*, 2005] and Oman [*Fleitmann et al.*, 2003] that both show around one per mille depletion at ~6 kya BP. Seasonally, the depletion extends slightly further north in January than in July (when temperatures are slightly warmer). In northern Africa, there is a large depletion signal, which is similar to that recorded in paleowaters of the region [*Gasse*, 2000].

[44] Neither the spatial patterns of NAM/SAM or tropical SST variability nor the amplitude of effects appears significantly different to the PI simulations. The SAM explains slightly more variance in the MH simulations (34% compared with 31%) but the regression patterns of NAM and SAM to the isotope fields are extremely robust to the climate change. There is a strong projection of the mean SLP changes in the Southern Hemisphere onto the SAM pattern, with the MH climate having a significantly more negative phase. This is due to a decrease in SLP in the Northern Hemisphere as a result of the asymmetric warming that must correspond to an increase in atmospheric mass (and SLP) in the south. This pattern of behavior where the SAM mode appears to respond to interhemispheric mass transports was also seen in freshwater forcing experiments with an earlier GISS model [*Rind et al.*, 2001].

6. Isotope-Climate Relationships

[45] In the preceding sections, we have shown that isotopes in precipitation and seawater follow predictable patterns of climate variability both for intrinsic and the selected forced climate changes. However, the fundamental paleoclimatic challenge is to invert any particular isotopic record to infer the climate change, but to do so, the relationship in time between the isotope record and the specific climate change must be known.

[46] Temporal relationships can be calculated from our results in a number of ways. Most simply, we can calculate the local correlations between the isotopes and relevant climate variables in the coupled model at different timescales for the full time series as shown in Figure 8. However, this could be distorted by the relative strength of different sources of variability in the model compared to the real world. A second method is to look at the temporal relationships for specific types of climate variability (such as described in section 4) and to deduce the relative changes in the isotopes associated with each of those patterns. To the extent that these patterns represent realistic teleconnections, these individual relationships should be more robust when applied to the real world.

6.1. $\delta^{18}O_p$ and Temperature/Precipitation

[47] The local temporal relationship between $\delta^{18}O_p$ and SAT ($\Delta\delta^{18}O_p/\Delta T$) and precipitation ($\Delta\delta^{18}O_p/\Delta P$) for interannual internal variability in the coupled model is usually

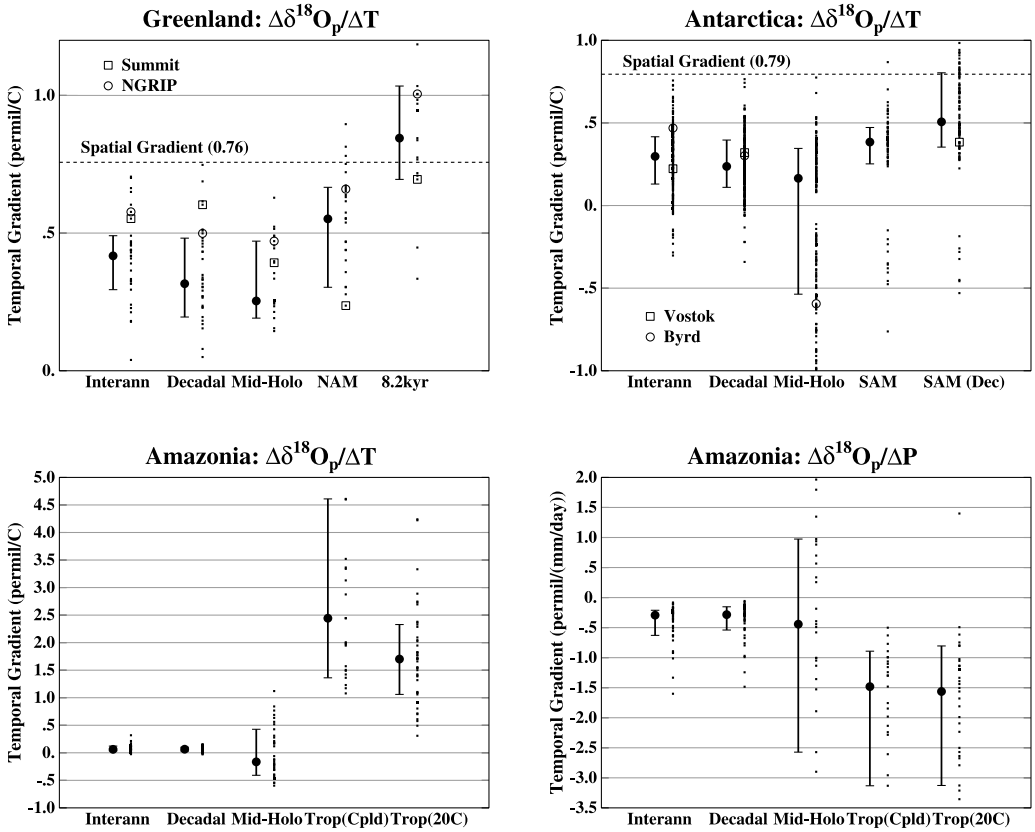

Figure 9. Local isotope-SAT gradients for three regions (Greenland, Antarctica, and Amazonia) and isotope-precipitation gradient for Amazonia for a selection of relevant climate processes: interannual intrinsic variability, decadal mean intrinsic variability, PI to MH differences, NAM- and SAM-related changes, NADW changes (associated with 8.2 kyr event experiments [*LeGrande et al.*, 2006]), and tropical SST variability in the coupled model and in the twentieth-century experiments with observed transient SST fields. Each dot represents an individual grid point where there is a correlation between the fields of at least 95% significance. The ranges are the 20th and 80th percentiles of all significant regional gradients. For reference, the modelled spatial gradients over each ice sheet are indicated (dashed horizontal lines).

thought of as the key to interpreting the isotopic records. As seen in previous work, correlations at both interannual (Figure 8) and interdecadal (not shown) timescales are positive to temperature in the mid-to-high latitudes and negative to precipitation, particularly in the tropics [e.g., *Cole et al.*, 1993; *Hoffmann et al.*, 1998; *Noone and Simmonds*, 2002]. Although these relationships are robust for all the internal variability, they are not necessarily a good predictor of the isotope signal associated with specific modes of variability (NAM, SAM, etc.) or for large-scale changes on millennial timescales such as the mid-Holocene. We therefore show the distribution of temporal gradients for different continental regions to quantify potential changes in these relationships as a function of relevant climate changes.

[48] We highlight variability in isotope-climate relationships in three regions relevant to paleoclimate ice-core interpretations: Greenland, Antarctica, and Amazonia (for the Andean ice cores). For each region, we calculate the grid-box $\delta^{18}O_p$/temperature (and $\delta^{18}O_p$/precipitation for Amazonia) relationships for the full spectrum of internal variability (as in Figure 8) and for changes associated with NAM, SAM, the MH (orbital), North Atlantic, and tropical variability. Since responses are generally regionally coherent, we calculate the mean temporal gradient for the region and the 20th and 80th percentiles for that gradient (including only the grid boxes that have correlations which are significant at >95%) (Figure 9). Specific grid boxes that correspond to key ice-core locations are highlighted if a significant relationship was found. Given the resolution of the model, individual grid-box responses should not be assumed to be an accurate representation of the actual location, but collectively, they may be a useful guide.

[49] In Greenland (Figure 9a), intrinsic variations at interannual and decadal timescales give similar results (mean values of 0.3 and 0.4‰/°C). For the Summit (70°N 38°W) and the Northern Greenland Ice Core Program (NGRIP) (75°N 42°W) sites, values are higher than 0.5–0.6 and noticeably less than the spatial gradient (0.76), consistent with previous modelling [*Werner et al.*, 2000]. However, gradients associated with NAM-related variability vary more widely over the ice sheet, causing the greatest difference between NGRIP, with a clear isotopic response, and Summit, with a much weaker response. An even stronger response (~0.8‰/°C) is seen in the mean impact of NADW variations associated with experiments performed with this model for the 8.2-kyr event [*LeGrande*

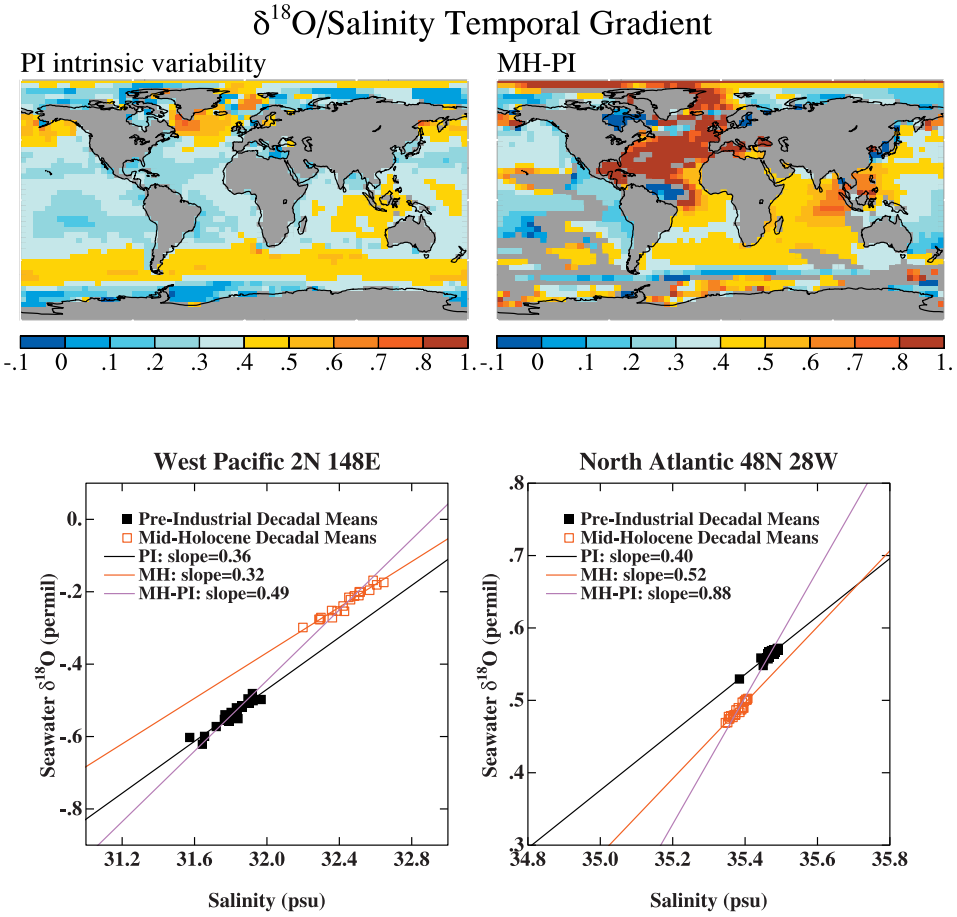

Figure 10. (a) Local regression of $\delta^{18}O_w$ to salinity over 200 years of intrinsic variability in the PI control. (b) The temporal gradient between the PI and MH simulations. (c) The relationship between $\delta^{18}O_w$ to salinity at selected individual points showing the variability in the MH and PI experiments.

et al., 2006]. Again, there are clear differences between the Summit and the NGRIP grid boxes.

[50] For Antarctica (Figure 9b), gradients related to interannual intrinsic variability are similar to the decadal signal with mean gradients of 0.2 and 0.3‰/°C, and as with Greenland, these are smaller than variations associated with variations in the SAM (0.4 to 0.5‰/°C). The spatial gradient across Antarctica is 0.8‰/°C (slightly greater than observed); however, the temporal gradients are significantly smaller than the estimates from previous models and data analyses (0.6–0.7‰/°C) for Vostok (78°S 107°E) and Dome C (75°S 123°E) [*Jouzel et al.*, 2003]. In the MH experiments where there is a slight cooling over the whole continent, there is a bimodel response between negative gradients around the edge of the continents (increases in $\delta^{18}O_p$ associated with increased divergence of sea ice and enhanced open water areas around the coast) and positive gradients in the more central areas. The Vostok results, however, show more consistency than is seen in general over the continent; nevertheless, it should be noted that both temperature and isotope changes for the MH are small, and thus ratios may not be robust.

[51] Amazonia has the biggest variations in isotope climate relationships. We show both the changes with respect to local temperature and local precipitation (Figures 9c and 9d). Interannual and decadal variability in temperature and precipitation gives rise to relatively small changes in the isotopic signal (~0.1‰/°C and approximately −0.3‰ mm^{-1} day^{-1}, respectively). However, the sensitivity of the isotopes to variations in temperature and precipitation specifically associated with tropical Pacific SST variability is much stronger. In both the coupled model and the twentieth-century simulations (which have an order of magnitude greater than the tropical Pacific variability), the local gradients are more than 2‰/°C and −1.5‰ mm^{-1} day^{-1}. At the MH, the local gradients are much more regionally variable as a function of the shifts in the ITCZ.

6.2. $\delta^{18}O_w$ and Salinity

[52] Analogous to the atmospheric relationships, we can assess the $\delta^{18}O_w$/S temporal gradient by looking at intrinsic variability, the forced changes in the MH, and the 8.2-kyr simulations. For this analysis, we only consider decadal and longer changes because of the coarser time resolution generally available in ocean records (although corals are a significant exception).

[53] In the analysis of intrinsic variability, we see very strong correlations between $\delta^{18}O_w$ and salinity everywhere in the open ocean—with the exception of the Arctic regions (due to the complicating sea ice factor). As might be expected from the spatial gradients, the temporal gradients

(Figure 10a) are steeper in the mid- to high latitudes (~0.5‰/psu) and shallower (in general) in the tropics (0.2–0.4‰/psu). One exception to this pattern is the West Pacific warm pool/Indian Ocean region, where the gradients are slightly steeper than in the rest of the tropical ocean (>0.4‰/psu), possibly due to that region's central role in exporting water vapor to the extratropics.

[54] The temporal gradients derived from the intrinsic variability in the MH simulations are qualitatively similar to that seen in the PI. However, the gradient between the PI and the MH is significantly different (Figure 10b). In the North Atlantic, the $\Delta\delta^{18}O_w/\Delta S$ ranges from 0.8 to 1.2‰/psu and 0.6 to 0.8‰/psu in the West Pacific—in both cases, twice as steep as seen in the intrinsic variability (Figure 10c). However, at other points (such as the East Pacific), the MH and PI points mostly overlap. The differences are likely due to the water vapor flux changes out of the tropics and, in particular, out of the Pacific. The freshwater end-member (−16‰) for these changes is some weighted mean atmospheric vapor value, which is more depleted than the pure evaporate, and thus causes a steepening of the $\delta^{18}O_w/S$ temporal gradient for the West Pacific. For the North Atlantic temporal shift, the freshwater end-member is even more depleted (−30‰), reflecting further rainout of the anomalous tropical vapor. Some shifts in ocean transports may also play a role here.

[55] For NADW variations associated with the 8.2 kyr simulations (not shown), the North Atlantic temporal gradient is 0.7 to 0.9‰/psu. The steepening of the gradient in those freshwater forcing experiments is in part a function of the depleted meltwater (−30‰), along with an associated sea ice effect, which makes the effective freshwater end-member significantly lighter than in the intrinsic variability [*LeGrande et al.*, 2006].

7. Controls on d-excess Records

[56] In contrast to $\delta^{18}O_p$, d-excess is generally assumed to have a strong nonlocal interpretation. It is therefore useful to supplement the results shown in the previous sections with direct correlations of the d-excess records from the ice coring regions of Greenland and Antarctica with more regional climate changes.

7.1. Vostok

[57] We correlate the d-excess signal at the Vostok grid box with larger-scale patterns, in particular, the SLP and SST fields (Figure 11). We find that the correlations with SST variability are quite subdued although in support of some previous simpler models, there is a positive correlation across a broad band of SST in the SH subtropical gyres [*Petit et al.*, 1991]. However, we find a large component of variability related to SAM (Figure 11). The d-excess signal is negatively correlated with the strength of the westerly winds [i.e., a bigger d-excess occurs when winds (and local evaporation) are least and there is more onshore advection]. This SAM-related variability dominates the local temperature correlation, and in the model forces, a positive d-excess/local temperature in contrast to the negative correlation is expected from the parcel models [*Ciais et al.*, 1994; *Vimeux et al.*, 2001]. This prediction of the model should be amenable to testing from the network of high-resolution shallow ice cores that are being processed as part of the ongoing International Trans-Antarctic Scientific Expedition project [*Steig et al.*, 2005].

[58] Changes at the MH are coherent across the continent (Figure 12). Despite the climatological bias at Vostok (~5°C too warm, 50‰ in too enriched), the points that approach Vostok conditions clearly converge toward a change in d-excess that is consistent with the observed change [*Vimeux et al.*, 2001]. Interestingly, the MH shift toward the more negative SAM in this model should produce a slight increase in d-excess (by about 0.4‰), but this tendency is overwhelmed by the larger "nonlocal" component related to the reduced equator to the pole SST gradient.

7.2. Greenland Summit

[59] The results for the Summit d-excess (Figure 13) agree more with the standard interpretation. There is a negative local correlation with temperature and a positive correlation to subtropical SST. However, as with the Southern Hemisphere records, there is a strong dependence on an SLP pattern associated with the annular modes. Interestingly, it is of the opposite sign to that in the Southern Hemisphere, probably related to the "upstream" conditions in Greenland compared with the "downstream" conditions in Antarctica and Eurasia. The pattern of SST correlations is similar as well to that associated with NAM variability, and so it may well be that the annular modes are the fundamental controls on d-excess—at least on these timescales and in this model. Given that the impact of NAM changes sign over the center of the ice sheet, it suggests why d-excess changes on short timescales do not appear to correlate between Summit and NGRIP (320 km to the north of Summit) [*Masson-Delmotte et al.*, 2005].

[60] At the MH, there is a small but variable signal over Greenland (±0.3‰), consistent with a lack of any significant millennial trends in the observed records. However, at the 8.2-kyr event, the observed changes at GRIP are significant (around −1.5‰) but are small and unclear at NGRIP [*Masson-Delmotte et al.*, 2005]. Our modelled changes (consistent with a 60% decrease in NADW at that time) are smaller (a decrease of about 0.6‰ at GRIP, no significant change at NGRIP) with stronger signals toward the southern end. It is unclear whether the observed differences in the ice cores are climatically significant or whether model biases over Greenland (poorly resolved inversion layers, excessive accumulation, insufficient sensitivity in temperature, etc.) may be important. Future work with higher-resolution models will be needed to assess this.

8. Discussion

[61] Water isotopes faithfully record changes in the climate systems for all the sources of variability discussed in this paper. However, our results point to a greater variability in their relationship to climate than previously assumed. These first results from coupled isotope-enabled models highlight the importance of understanding the spatial patterns of proxy variability in the past.

[62] We assessed many kinds of climate changes relevant to the Holocene, including intrinsic variations and changes driven by orbital, freshwater, and tropical SST forcings. The

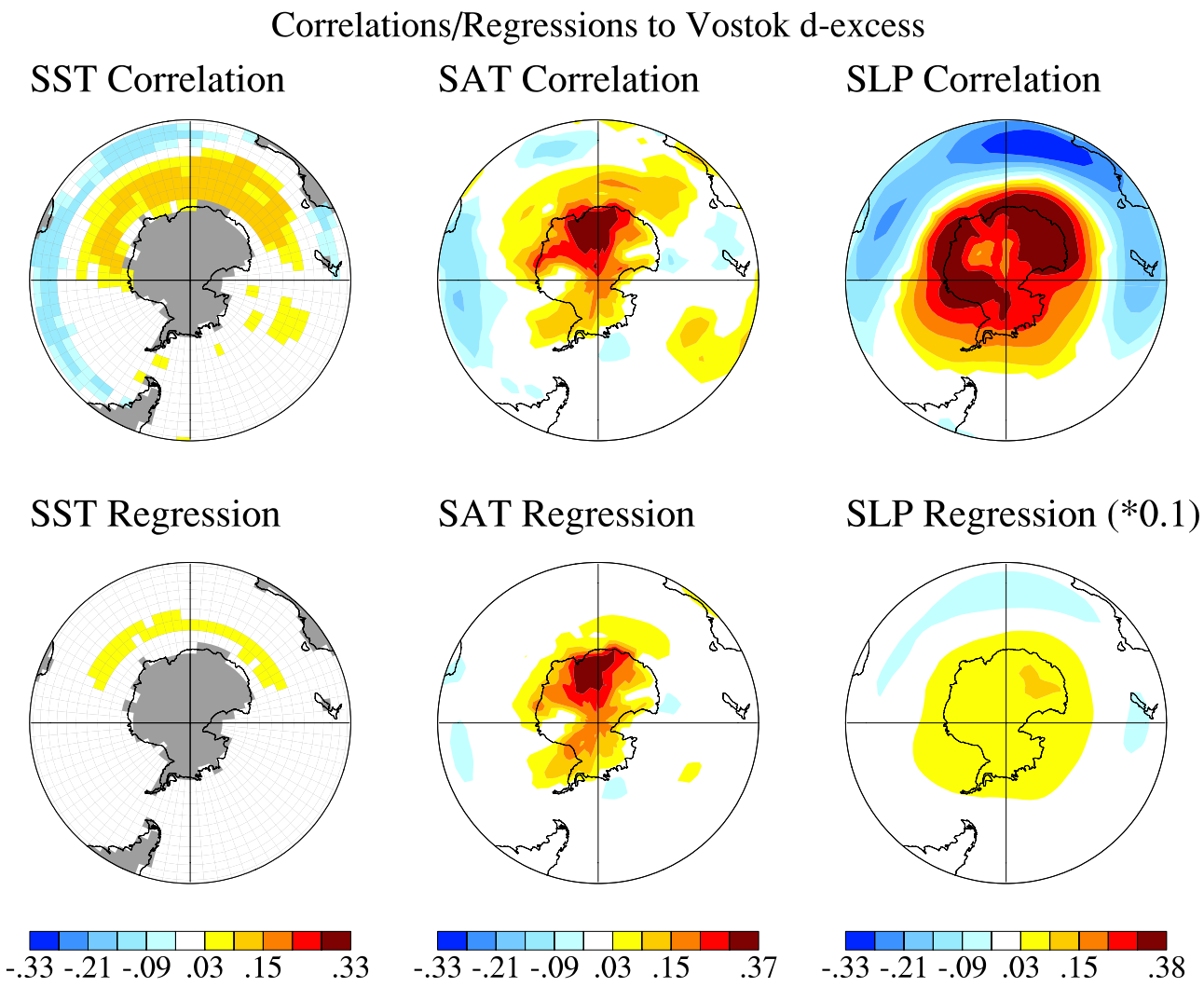

Figure 11. Correlations and regressions of interannual d-excess variability at Vostok compared to SST, SAT, and SLP. Correlations are highest for the SLP changes (which in turn are highly correlated to the SAM index).

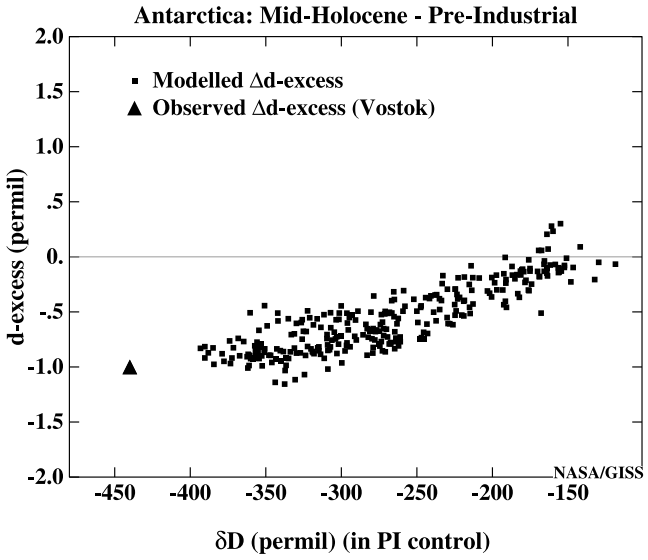

Figure 12. Changes in d-excess at the MH for all points in Antarctica compared to observations at Vostok.

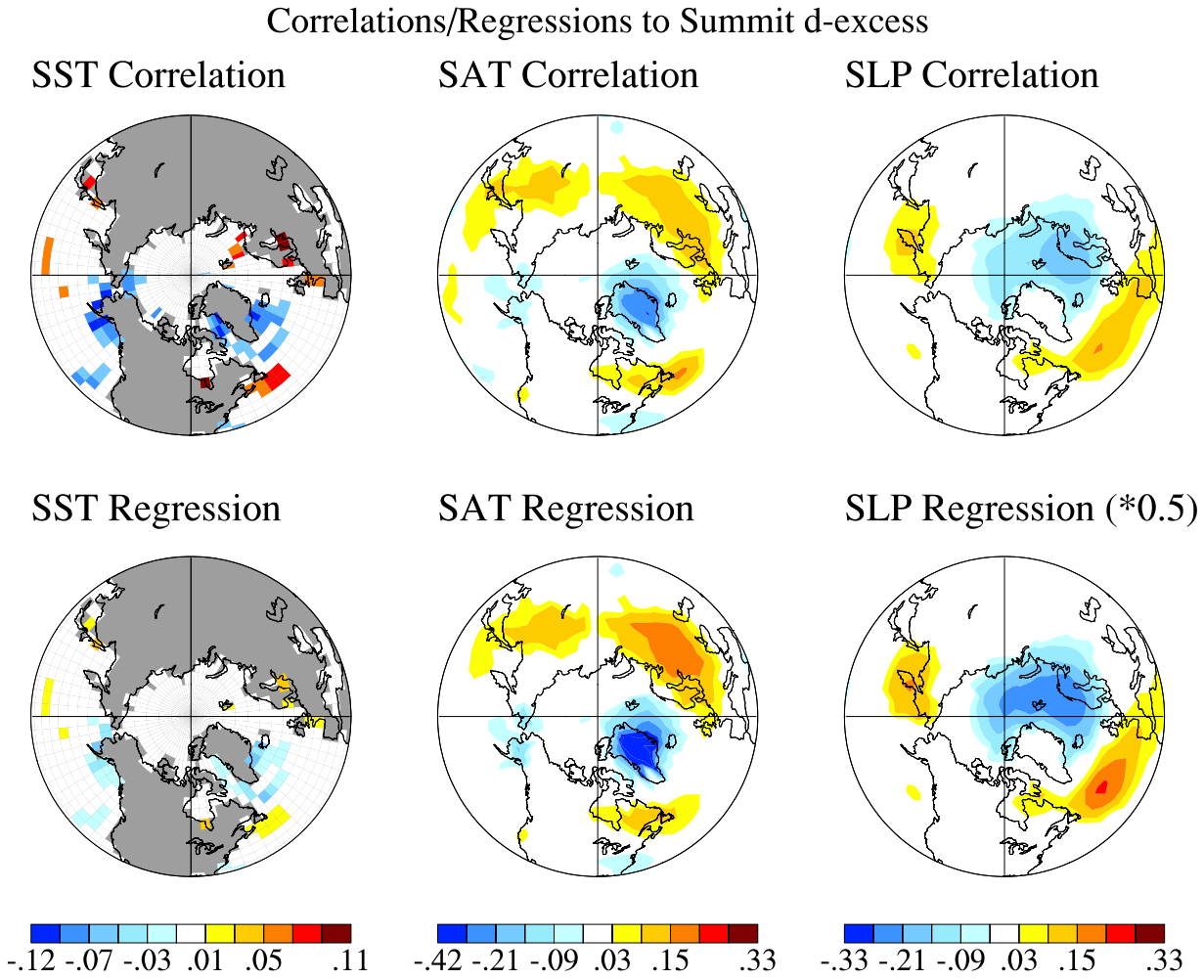

Figure 13. Correlations and regressions of interannual d-excess variability at Summit compared to SST, SAT, and SLP.

isotopes do, in general, record important climate changes. However, we find little evidence for a unique quantitative local relationship between any isotopic record and a particular climate variable. Specifically, over different timescales, and with different forcings, the relationships vary by large factors—more so in the precipitation-dominated tropics than in the temperature-controlled high latitudes—but in all cases, they vary enough to substantially increase error bars on locally calibrated isotopic climate reconstructions. As in previous work, the spatial gradients are not found to be good predictors of temporal gradients on any timescale.

[63] In the atmosphere, changes in seasonality [*Werner et al.*, 2000], transport pathways [*Charles et al.*, 1994], tropical export, or cross-isthmus export of freshwater and with concomitant variations in isotopic content are almost certainly implicated in the wide variation of results seen here.

[64] In the ocean, the results indicate that the end-members of the mixing lines in intrinsic interdecadal variability are different to the net freshwater and isotope transport changes that occur when the whole system moves to a new state. This can involve both changes in the atmospheric water vapor fluxes and in the ocean transports. Work is ongoing to better quantify those changes for the MH.

[65] What evidence is there that these nonstationary local relationships are real phenomena as opposed to a model-specific result? Errors in climatology in the models (for example, too warm Antarctic plateau, insufficient vertical resolution to simulate winter inversion layers over the ice sheets, etc.) could bias some of the results, but this remains unquantified at this point. Clearly, further experiments with different isotope-enabled coupled models will be useful in solidifying these results [development of analogous Hadley Center and NCAR CSM modules is ongoing (J. Tindall and D. Noone, personal communication, 2006)], but there is support for these general conclusions even from the observational data. For instance, *Landais et al.* [2004] conclude that $\delta^{18}O_p$-T relationships over Dansgaard-Oeschger events in the NGRIP core are temporally varying, and correlations of GRIP isotopes to the borehole temperature record [*Dahl-Jensen et al.*, 1998] do not demonstrate the same sensitivity for the last millennia than for the glacial-interglacial changes.

[66] If these results are robust, they should be taken as implying that isotope-based records contain a more sophisticated detail of climate history and thus require a slightly more complex analysis to interpret than used to date. Indeed, the isotopic signatures of climate variability in our

simulations are very clear and suggest strongly that more "nonlocal" interpretations should be sought. This could involve point calibrations to larger-scale phenomena (such as movements of the ITCZ, or the export of tropical water vapor) or combining of different records to produce a spatial pattern of isotope change that could be more easily associated with the patterns seen in sections 4 and 5. Examples of this approach exist, for instance, for the 8.2-kyr event [*Rohling and Pälike*, 2005], and modelling attempts to match the isotopic pattern directly have been relatively successful [*LeGrande et al.*, 2006].

[67] In the tropics, examples for Andean and Himalayan ice core signals [*Hoffmann et al.*, 2003; *Vuille et al.*, 2005] and corals [*Brown et al.*, 2006] are available. Additionally, the pattern of response to MH forcing seen in this paper shows a good match to the direct isotopic data. One clear conclusion from our results is that the isotopic response is significantly more regionally homogenous than the precipitation anomalies. Thus isotopic records are likely to be less affected by local microclimate effects than a direct precipitation record might be and are thus more useful at capturing regional-scale climatic phenomena.

[68] **Acknowledgments.** The support for GAS and ANL was provided from NSF grants OCE-99-05038 and ATM-05-01241. Assistance for GAS from EGIDE and CEA France during the numerous visits to Saclay is also gratefully acknowledged. A support for ANL was also provided from an NDSEG graduate student fellowship. We thank three anonymous reviewers who helped significantly improve the clarity of the manuscript.

References

Aharon, P., and J. Chappell (1986), Oxygen isotopes, sea-level changes and the temperature history of a coral-reef environment in New Guinea over the last 105 years, *Palaeogeogr. Palaeoclimatol. Palaeoecol.*, *56*, 337–379.

Aleinov, I., and G. A. Schmidt (2006), Water isotopes in the GISS ModelE land surface scheme, *Glob. Planet. Change*, *51*, 108–120.

Berger, A. (1978), Long-term variations of daily insolation and Quaternary climatic changes, *J. Atmos. Sci.*, *35*, 2362–2367.

Braconnot, P., S. Joussaume, O. Marti, and N. de Noblet (1999), Synergistic feedbacks from ocean and vegetation on the African monsoon response to mid-Holocene insolation, *Geophys. Res. Lett.*, *26*, 2481–2484.

Bradley, R. S., M. Vuille, D. Hardy, and L. G. Thompson (2003), Low latitude ice cores record Pacific sea surface temperatures, *Geophys. Res. Lett.*, *30*(4), 1174, doi:10.1029/2002GL016546.

Bretherton, J., and D. Battisti (2000), An interpretation of the results from atmospheric general circulation models forced by the time history of the observed sea surface temperature distribution, *Geophys. Res. Lett.*, *27*, 767–770.

Brown, J., I. Simmonds, and D. Noone (2006), Modeling $\delta^{18}O$ in tropical precipitation and the surface ocean for present-day climate, *J. Geophys. Res.*, *111*, DO5105, doi:10.1029/2004JD005611.

Brutsaert, W. H. (1982), *Evaporation Into the Atmosphere*, Springer, New York.

Cappa, C. D., M. Hendricks, D. J. DePaolo, and R. C. Cohen (1993), Isotopic fractionation of water during evaporation, *J. Geophys. Res.*, *108*, 4525, doi:10.1029/2003JD003597.

Charles, C. D., D. Rind, J. Jouzel, R. D. Koster, and R. G. Fairbanks (1994), Variable air mass sources for Greenland: Influences on the ice core record, *Science*, *263*, 508–511.

Ciais, P., J. Jouzel, J. R. Petit, V. Lipenkov, and J. W. C. White (1994), Holocene temperature variations inferred from six Antarctic ice cores, *Ann. Glaciol.*, *20*, 427–436.

Cole, J. E., D. Rind, and R. G. Fairbanks (1993), Isotopic responses to interannual climate variability simulated by an atmospheric general circulation model, *Quat. Sci. Rev.*, *12*, 387–406.

Cole, J. E., D. Rind, R. S. Webb, J. Jouzel, and R. Healy (1999), Climatic controls on interannual variability of precipitation $\delta^{18}O$: Simulated influence of temperature, precipitation amount, and vapor source region, *J. Geophys. Res.*, *104*, 14,223–14,235.

Craig, H., and L. I. Gordon (1965), Deuterium and oxygen 18 variations in the ocean and the marine atmosphere, in *Stable Isotopes in Oceanographic Studies and Paleotemperatures*, edited by E. Tongiorgi, pp. 9–130, Cons. Naz. di Rech., Spoleto, Italy.

Dahl-Jensen, D., K. Mosegaard, N. Gundestrup, G. D. Clow, S. J. Johnsen, A. W. Hansen, and N. Balling (1998), Past temperatures directly from the Greenland ice sheet, *Science*, *282*, 268–271.

Dansgaard, W. (1964), Stable isotopes in precipitation, *Tellus*, *16*, 436–468.

Del Genio, A. D., M. S. Yao, W. Kovari, and K. K. Lo (1996), A prognostic cloud water parameterization for general circulation models, *J. Clim.*, *9*, 270–304.

Del Genio, A. D., W. Kovari, M.-S. Yao, and J. Jonas (2005), Cumulus microphysics and climate sensitivity, *J. Clim.*, *18*, 2376–2387.

Delaygue, G., J. Jouzel, and J.-C. Dutay (2000), Salinity-oxygen 18 relationship simulated by an oceanic general circulation model, *Earth Planet. Sci. Lett.*, *178*, 118–138.

Duplessy, J.-C. (1970), Note preliminaire sur les variations de la composition isotopique des eaux superficelles de l'Océan Indien: La relation ^{18}O-salinité, *C. R. Acad. Sci. Paris*, *271*, 1075–1078.

Duplessy, J.-C., E. Bard, L. Labeyrie, J. Duprat, and J. Moyes (1993), Oxygen isotope records and salinity changes in the Northeastern Atlantic Ocean during the last 18,000 years, *Paleoceanography*, *8*, 341–350.

Etheridge, D. M., L. P. Steele, R. L. Langenfelds, R. J. Francey, J. M. Barnola, and V. I. Morgan (1996), Natural and anthropogenic changes in atmospheric CO_2 over the last 1000 years from air in Antarctic ice and firn, *J. Geophys. Res.*, *101*, 4115–4128.

Fleitmann, D., S. J. Burns, M. Mudelsee, U. Neff, J. Kramers, A. Mangini, and A. Matter (2003), Holocene forcing of the Indian monsoon recorded in a stalagmite from Southern Oman, *Science*, *300*, 1737–1739.

Fröhlich, K., J. Grabczak, and K. Rozanski (1988), Deuterium and oxygen-18 in the Baltic Sea, *Chem. Geol.*, *72*, 77–83.

Gasse, F. (2000), Hydrological changes in the African tropics since the Last Glacial Maximum, *Quat. Sci. Rev.*, *19*, 189–211.

Gat, J. R., A. Shemesh, E. Tziperman, A. Hecht, D. Georgopoulos, and O. Basturk (1996), The stable isotope composition of waters of the eastern Mediterranean Sea, *J. Geophys. Res.*, *101*, 6441–6451.

Gent, P. R., and J. C. McWilliams (1990), Isopycnal mixing in ocean circulation models, *J. Phys. Oceanogr.*, *20*, 150–155.

Hansen, J. E., et al. (2005), Efficacy of climate forcings, *J. Geophys. Res.*, *110*, DI8104, doi:10.1029/2005JD005776.

Hansen, J. E., et al. (2002), Climate forcings in Goddard Institute for Space Studies SI2000 simulations, *J. Geophys. Res.*, *107*(D18), 4347, doi:10.1029/2001JD001143.

Hewitt, C. D., and J. F. B. Mitchell (1998), A fully coupled GCM simulation of the climate of the mid-Holocene, *Geophys. Res. Lett.*, *25*, 361–364.

Hoffmann, G. (2003), Taking the pulse of the tropical water cycle, *Science*, *301*, 776–777.

Hoffmann, G., M. Werner, and M. Heimann (1998), The water isotope module of the ECHAM Atmospheric General Circulation Model - A study on time scales from days to several years, *Journal of Geophysical Research*, *103*, 16,871–16,896.

Hoffmann, G., et al. (2003), Coherent isotope history of Andean ice cores over the last century, *Geophys. Res. Lett.*, *30*(4), 1179, doi:10.1029/2002GL014870.

Huffman, G. J., et al. (1997), The Global Precipitation Climatology Project (GPCP) combined precipitation data set, *Bull. Am. Meteor. Soc.*, *78*, 5–20.

Indermuhle, A., et al. (1999), Holocene carbon-cycle dynamics based on CO_2 trapped in ice at Taylor Dome, Antarctica, *Nature*, *398*, 121–126.

International Atomic Energy Agency (2001), GNIP maps and animations, International Atomic Energy Agency, Vienna. http://isohis.iaea.org.

Israelson, C., and B. Buchardt (1999), Strontium and oxygen isotope composition of East Greenland rivers and surface waters: Implication for palaeoenvironmental interpretation, *PPP*, *153*, 93–104.

Jacobs, S. S., R. G. Fairbanks, and Y. Horibe (1985), Origin and evolution of water masses near the Antarctic continental margin: Evidence from $H_2^{18}O/H_2^{16}O$ ratios in seawater, in *Oceanology of the Antarctic Continental Shelf*, edited by S. S. Jacobs, vol. 43 of Antarctic Res. Ser., pp. 59–85, AGU, Washington, D.C.

Joussaume, S., and J. Jouzel (1993), Paleoclimatic tracers: An investigation using an atmospheric general circulation model under ice age conditions: 2. Water isotopes, *J. Geophys. Res.*, *98*, 2807–2830.

Joussaume, S., et al. (1999), Monsoon changes for 6000 years ago: Results of 18 simulations from the Paleoclimate Modeling Intercomparison Project (PMIP), *Geophys. Res. Lett.*, *26*, 859–862.

Jouzel, J., G. L. Russell, R. J. Suozzo, R. D. Koster, J. W. C. White, and W. S. Broecker (1987), Simulations of HDO and $H_2^{18}O$ atmospheric cycles using the NASA GISS general circulation model: The seasonal cycle for present-day conditions, *J. Geophys. Res.*, *92*, 14,739–14,760.

Jouzel, J., R. D. Koster, R. J. Suozzo, G. L. Russell, J. W. C. White, and W. S. Broecker (1991), Simulations of HDO and $H_2^{18}O$ atmospheric cycles using the NASA GISS general circulation model: Sensitivity experiments for present-day conditions, *J. Geophys. Res.*, *96*, 7495–7507.

Jouzel, J., F. Vimeux, N. Caillon, G. Delaygue, G. Hoffmann, V. Masson-Delmotte, and F. Parrenin (2003), Magnitude of isotope/temperature scaling for interpretation of central Antarctic ice cores, *J. Geophys. Res.*, *108*(D12), 4361, doi:10.1029/2002JD002677.

Khatiwala, S. P., R. G. Fairbanks, and R. W. Houghton (1999), Freshwater sources to the coastal ocean off northeastern North America: Evidence from $H_2^{18}O/H_2^{16}O$, *J. Geophys. Res.*, *104*, 18,241–18,255.

Kushnir, Y., W. A. Robinson, I. Blade, N. M. J. Hall, S. Peng, and R. Sutton (2002), Atmospheric GCM response to extratropical SST anomalies: Synthesis and evaluation, *J. Clim.*, *15*, 2233–2256.

Landais, A., J. M. Barnola, V. Masson-Delmotte, J. Jouzel, J. Chappellaz, N. Caillon, C. Huber, M. Leuenberger, and S. J. Johnsen (2004), A continuous record of temperature evolution over a sequence of Dansgaard-Oeschger events during Marine Isotopic Stage 4 (76 to 62 kyr BP), *Geophys. Res. Lett.*, *31*, L22211, doi:10.1029/2004GL021193.

Large, W. G., J. C. McWilliams, and S. C. Doney (1994), Oceanic vertical mixing: A review and a model with non-local boundary layer parameterization, *Rev. Geophys.*, *32*, 363–403.

LeGrande, A. N., and G. A. Schmidt (2006), Global gridded dataset of the oxygen isotopic composition in seawater, *Geophys. Res. Lett.*, *33*, LI2604, doi:10.1029/2006GL026011.

LeGrande, A. N., G. A. Schmidt, D. T. Shindell, C. Field, R. L. Miller, D. Koch, G. Faluvegi, and G. Hoffmann (2006), Consistent simulations of multiple proxy responses to an abrupt climate change event, *Proc. Natl. Acad. Sci. U. S. A.*, *103*, 837–842.

Levitus, S., R. Burgett, and T. P. Boyer (1994), World ocean atlas 1994, *Tech. rep.*, U.S. Department of Commerce, Washington, D.C.

Liu, J., G. A. Schmidt, D. G. Martinson, D. Rind, G. L. Russell, and X. Yuan (2003), Sensitivity of sea ice to physical parameterisations in the GISS global climate model, *J. Geophys. Res.*, *108*(C2), 3053, doi:10.1029/2001JC001167.

Liu, Z., E. Brady, and J. Lynch-Stieglitz (2000), Modeling climate shift of El Niño variability in the Holocene, *Geophys. Res. Lett.*, *27*(15), 2265–2268, doi:10.1029/2000GL011452.

Lynch-Stieglitz, M. (1994), The development and validation of a simple snow model for the GISS GCM, *J. Clim.*, *7*, 1842–1855.

Macdonald, R. W., E. C. Carmack, E. C. McLaughlin, K. K. Falkner, and J. H. Swift (1999), Connections among ice, runoff and atmospheric forcing in the Beaufort Gyre, *Geophys. Res. Lett.*, *26*, 2223–2226.

Masson-Delmotte, V., et al. (2005), Holocene climatic changes in Greenland: Different deuterium excess signals at Greenland Ice Core Project (GRIP) and NorthGRIP, *J. Geophys. Res.*, *110*, DI4102, doi:10.1029/2004JD005575.

Meredith, M. P., K. J. Heywood, R. D. Frew, and P. F. Dennis (1999), Formation and circulation of the water masses between the Southern Indian Ocean and Antarctica: Results from $\delta^{18}O$, *J. Mar. Res.*, *57*, 449–470.

Merlivat, L., and J. Jouzel (1979), Global climatic interpretation of the deuterium-oxygen 18 relationship for precipitation, *J. Geophys. Res.*, *84*, 5029–5033.

Miller, R. L., G. A. Schmidt, and D. T. Shindell (2006), Forced annular variations in the 20th century Intergovernmental Panel on Climate Change Fourth Assessment Report models, *J. Geophys. Res.*, *111*, DI8101, doi:10.1029/2005JD006323.

Noone, D., and I. Simmonds (2002), Associations between $\delta^{18}O$ of water and climate parameters in a simulation of atmospheric circulation 1979–1995, *J. Clim.*, *15*, 3150–3169.

Östlund, H. G., H. Craig, W. S. Broecker, and D. Spenser (1987), GEOSECS Atlantic, Pacific and Indian Ocean expeditions: Shorebased Data and Graphics, vol. 7, *Tech. rep.*, National Science Foundation, Washington, D. C.

Paul, A., S. Mulitza, J. Pätzold, and T. Wolff (1999), Simulation of oxygen isotopes in a global ocean model, in *Use of Proxies in Paleoceanography: Examples From the South Atlantic*, edited by G. Fischer and G. Wefer, pp. 655–686, Springer, New York.

Petit, J. R., J. W. C. White, N. W. Young, J. Jouzel, and Y. S. Korotkevich (1991), Deuterium excess in recent Antarctic snow, *J. Geophys. Res.*, *96*, 5113–5122.

Prather, M. J. (1986), Numerical advection by conservation of second order moments, *J. Geophys. Res.*, *91*, 6671–6680.

Prentice, I. C., and T. Webb III (1998), BIOME 6000: Reconstructing global mid-Holocene vegetation patterns from palaeoecological records, *J. Biogeogr.*, *25*, 997–1005.

Rayner, N. A., D. E. Parker, E. B. Horton, C. K. Folland, L. V. Alexander, D. P. Rowell, E. C. Kent, and A. Kaplan (2003), Global analyses of SST, sea ice and night marine air temperature since the late nineteenth century, *J. Geophys. Res.*, *108*(D14), 4407, doi:10.1029/2002JD002670.

Rind, D., G. L. Russell, G. A. Schmidt, S. Sheth, D. Collins, P. Demenocal, and J. Teller (2001), Effects of glacial meltwater in the GISS Coupled Atmosphere-Ocean Model: Part II. A bi-polar seesaw in Atlantic Deep Water production, *J. Geophys. Res.*, *106*, 27,355–27,366.

Rohling, E. J., and G. R. Bigg (1998), Paleosalinity and $\delta^{18}O$: A critical assessment, *J. Geophys. Res.*, *103*, 1307–1318.

Rohling, E. J., and H. Pälike (2005), Centennial-scale climate cooling with a sudden cold event around 8,200 years ago, *Nature*, *434*, 975–979.

Rosenzweig, C., and F. Abramopoulos (1997), Land surface model development for the GISS GCM, *J. Clim.*, *10*, 2040–2054.

Rozanski, K., L. Araguás-Araguás, and R. Gonfiantini (1993), Isotopic patterns in modern global precipitation, in *Climate Change in Continental Isotopic Records*, edited by P. K. S., et al., no. 78 in Geophys. Monogr. Ser., AGU, Washington, D. C.

Russell, G. L., and J. A. Lerner (1981), A new finite-differencing scheme for the tracer transport equation, *J. Appl. Meteorol.*, *20*, 1483–1498.

Russell, G. L., J. R. Miller, and D. Rind (1995), A coupled atmosphere-ocean model for transient climate change, *Atmos. Ocean*, *33*, 683–730.

Russell, G. L., J. R. Miller, D. H. Rind, R. A. Ruedy, G. A. Schmidt, and S. Sheth (2000), Comparison of model and observed regional temperature changes during the past 40 years, *J. Geophys. Res.*, *105*, 14,891–14,898.

Santer, B. D., et al. (2005), Amplification of surface temperature trends and variability in the tropical atmosphere, *Science*, *309*, 1551–1556.

Schmidt, G. A. (1998), Oxygen-18 variations in a global ocean model, *Geophys. Res. Lett.*, *25*, 1201–1204.

Schmidt, G. A. (1999a), Error analysis of paleosalinity calculations, *Paleoceanography*, *14*, 422–429.

Schmidt, G. A. (1999b), Forward modeling of carbonate proxy data from planktonic foraminifera using oxygen isotope tracers in a global ocean model, *Paleoceanography*, *14*, 482–497.

Schmidt, G. A., G. R. Bigg, and E. J. Rohling (1999), Global seawater oxygen-18 database, http://data.giss.nasa.gov/data/o18data.

Schmidt, G. A., C. M. Bitz, U. Mikolajewicz, and L. B. Tremblay (2004a), Ice-ocean boundary conditions for coupled models, *Ocean Model.*, *7*, 59–74.

Schmidt, G. A., D. T. Shindell, R. L. Miller, M. E. Mann, and D. Rind (2004b), General circulation modelling of Holocene climate variability, *Quat. Sci. Rev.*, *23*, 2167–2181, doi:10.1016/j.quascirev.2004.08.005.

Schmidt, G. A., G. Hoffmann, D. T. Shindell, and Y. Hu (2005), Modeling atmospheric stable water isotopes and the potential for constraining cloud processes and stratosphere-troposphere water exchange, *J. Geophys. Res.*, *110*, 021314, doi:10.1029/2005JD005790.

Schmidt, G. A., et al. (2006), Present day atmospheric simulations using GISS ModelE: Comparison to in-situ, satellite and reanalysis data, *J. Clim.*, *19*, 153–192, http://www.giss.nasa.gov/tools/modelE.

Schneider, D. P., E. J. Steig, T. D. van Ommen, D. A. Dixon, P. A. Mayewski, J. M. Jones, and C. M. Bitz (2006), Antarctic temperatures over the past two centuries from ice cores, *Geophys. Res. Lett.*, *33*, LI6707, doi:10.1029/2006GL027057.

Shindell, D. T., G. A. Schmidt, R. L. Miller, and D. Rind (2001), Northern hemisphere winter climate response to greenhouse gas, ozone, solar and volcanic forcing, *J. Geophys. Res.*, *106*, 7193–7210.

Steig, E. J., et al. (2005), High-resolution ice cores from US ITASE (West Antarctica): Development and validation of chronologies and determination of precision and accuracy, *Ann. Glaciol.*, *41*, 77–84.

Thompson, D. W. J., and J. M. Wallace (1998), The Arctic Oscillation signature in the wintertime geopotential height and temperature fields, *Geophys. Res. Lett.*, *25*, 1297–1300.

Toggweiler, J. R., and B. Samuels (1995), Effect of sea ice on the salinity of Antarctic bottom waters, *J. Phys. Oceanogr.*, *25*, 1980–1997.

Vimeux, F., V. Masson, J. Jouzel, J. R. Petit, E. J. Steig, M. Stievenard, R. Vaikmae, and J. W. C. White (2001), Holocene hydrological cycle changes in the southern hemisphere documented in East Antarctic deuterium excess records, *Clim. Dyn.*, *17*, 503–513.

Visbeck, M., J. Marshall, and T. Haine (1997), Specification of eddy transfer coefficients in coarse-resolution ocean circulation experiments, *J. Phys. Oceanogr.*, *27*, 381–402.

Vuille, M., R. S. Bradley, M. Werner, R. Healy, and F. Keimig (2003), Modeling $\delta^{18}O$ in precipitation over the tropical Americas: 1. Interannual variability and climatic controls, *J. Geophys. Res.*, *108*(D6), 4174, doi:10.1029/2001JD002038.

Vuille, M., M. Werner, R. S. Bradley, and F. Keimig (2005), Stable isotopes in precipitation in the Asian monsoon region, *J. Geophys. Res.*, *110*, D23108, doi:10.1029/2005JD006022.

Wajsowicz, R. C. (1993), A consistent formulation of the anisotropic stress tensor for use in models of the large-scale ocean circulation, *J. Comp. Physiol.*, *105*, 333–338.

Wang, Y., et al. (2005), The Holocene Asian monsoon: Links to solar changes and North Atlantic climate, *Science*, *308*, 854–857.

Weiss, R. F., H. G. Östlund, and H. Craig (1979), Geochemical studies of the Weddell Sea, *Deep Sea Res. Part A*, *26*, 1093–1120.

Werner, M., U. Mikolajewicz, M. Heimann, and G. Hoffmann (2000), Borehole versus isotope temperatures on Greenland: Seasonality does matter, *Geophys. Res. Lett.*, *27*, 723–726.

Xie, P., and A. Arkin (1997), Global precipitation: A 17-year monthly analysis based on gauge observations, satellite estimates, and numerical model outputs, *Bull. Am. Meteorol. Soc.*, *78*, 2539–2558.

Yao, M. S., and A. D. Del Genio (1989), Effects of cumulus entrainment and multiple cloud types on a January global climate model simulation, *J. Clim.*, *2*, 850–863.

Yobbi, D. K. (1992), Effects of tidal stage and ground-water levels on the discharge and water quality of springs in coastal Citrus and Hernando counties, Florida, *Tech. Rep. Water Resources Investigations Report 92–4096*, U.S. Geol. Surv.

Zhang, J., and D. Rothrock (2000), Modeling Arctic sea ice with an efficient plastic solution, *J. Geophys. Res.*, *105*, 3325–3338.

G. Hoffmann, Laboratoire des Sciences du Climat et de l'Environnement (LSCE), Orme des Merisiers F-91191, Gif-sur-Yvette, Cedex, France. (hoffmann@lsce.saclay.cea.fr)

A. N. LeGrande and G. A. Schmidt, NASA Goddard Institute for Space Studies and Center for Climate Systems Research, Columbia University, 2880 Broadway, New York, NY 10025, USA. (legrande@giss.nasa.gov; gschmidt@giss.nasa.gov)